8-2023

Modeling & Small Signal Analysis of Grid Forming Inverter

Kadesh Hepburn
University of Arkansas-Fayetteville

Modeling & Small Signal Analysis of Grid Forming Inverters

A thesis submitted in partial fulfilment
of the requirements for the degree of
Master of Science in Electrical Engineering

by

K'Adesh Hepburn
University of Arkansas
Bachelor of Science in Electrical Engineering, 2017

August 2023
University of Arkansas

This thesis is approved for recommendation to the Graduate Council.

_____
Roy McCann, Ph.D.
Thesis Director

_____
Jingxian Wu, Ph.D.
Committee Member

_____
Juan Carlos Balda, Ph.D.
Committee Member

ABSTRACT

There is a rising number of inverter-based resources (IBRs) being integrated with distribution systems are becoming a more common occurrence. With integration of IBRs inverters, power utilities are experiencing an increase of number of operations with regards to voltage and frequency support. To maintain grid stability and reliability, IBRs need to provide some of the services currently (or formerly) provided by synchronous generators. Interconnection standards, like the IEEE 1547. 2018 has include requirements for IBRs to have the capability to provide some of these services—such as frequency and voltage support—and the procurement and deployment of the services can be implemented either as mandatory interconnection requirements or as market products. All the IBRs deployed today are grid-following (GFL), and read the voltage and frequency of the grid and inject current to provide the appropriate amount of active and reactive power.

The fundamental GFL IBR design assumption is that there are still enough synchronous generators on the grid to provide a relatively strong and stable voltage and frequency signal, which GFL IBRs can "follow." But since levels of GFL are increasing, there will be a limit to how far GFL controls can be pushed, and, at some point, new advanced inverter controls (termed grid forming (GFM)) will be needed to maintain system stability. GFM IBRs will also be needed to establish voltage and frequency during operating conditions when there are zero synchronous machines (100 percent IBR penetration). Power systems around the world are at the point of now needing to make this technological leap; however, system operators and planners, equipment owners, and manufacturers today are facing a circular problem regarding the deployment of advanced IBR controls. Which comes first, the requirement for a capability or the capability itself? How do grid operators know what performance or capability is possible from new

equipment (and therefore what they could require)? How can they evaluate costs and benefits of having such equipment on the grid? What drives manufacturers to invest in modern technology without its being mandated for interconnection to the grid or otherwise incentivized by the market?

The objective of this thesis is to provide a better understanding of ride through fault capabilities of Grid Forming Inverter (GFM) tied into the generation side of the power grid when using control functions. Furthermore, to investigate the robustness of implementing time delay with a PLL system within the control settings for grid forming inverters. To this end, to identify the contributing factors that affects the stability of the time delay to better design and future models of GFMs. As discussed, the microgrid is a potential solution for future distributed generation systems. However, controlling a microgrid is still a complex issue and many proposed solutions, are only based on locally measured signals without any communications; thus, it is difficult to achieve global optimization. Future works on this topic will analyse the role of restoration practices, communication control techniques to better approximate the delay. The specific areas below will be discussed in this thesis.

ACKNOWLEDGEMENTS

I would like to thank Dr. Roy McCann for all the support, teaching and inspiration throughout my master's journey. I also would like to thank Mr. Saunders for his continues wisdom and guidance on this journey and giving me the opportunity to work alongside a great group of individuals.

I would also like to thank Dr. Juan C. Balda for his technical knowledge he had provided in my lectures and practical application which helped me appreciate the work and overall implementation with the various power electronics devices. Along with a shared passion for power distribution systems.

I also would like to thank Dr. Jingxian Wu for serving on my Master committee and sharing his knowledge and experience in his communication class, which provided the fundamental framework, appreciation and usefulness for this topic.

I would like to extend gratitude to Mr. Mojitaba Ahanch, who provided me insightful knowledge and tip on the various power simulation software and was always happy to share his knowledge with me.

Lastly, this journey was heartful and couldn't be made possible without the support of my friends and family. I would like to thank my wife, Jessica Marc, for being my rock and giving me her continuous love and support. Also, to my parents and brothers for their continuous support throughout my entire academic career.

TABLE OF CONTENTS

CHAPTER 1

INTRODUCTION

1.1 Motivations for this Research Work 1

1.2 Why a Grid Forming Inverters?…….....….3

1.3 Grid Interaction capabilities of GFL and GFM.....4

1.3.1 Volt/VAr Function 3

1.3.2 Fixed Power Factor Function 4

1.3.3 Dynamic reactive current function 4

1.4 Grid Forming Inverter (GFM) Controller Functions.....7

1.4.1 Droop Controller…..... 8

1.4.2 Active Power-Frequency Droop Control..... 12

1.4.3 Reactive Power-Voltage Droop Control..... 12

1.4.4 Phase Lock Loop……..... 12

1.4.5 Voltage Controller……..... 13

1.4.6 Current Controller……..... 13

1.4.7 Time Delay Model……..... 13

1.5 Objectives of Thesis 14

1.6 Organization of Thesis 15

CHAPTER 2

LITERATURE SURVEY

2.1 Introduction 18

2.2 Stability concerns in Grid Forming Inverter 19

2.2.1 Frequency Stability 19

2.2.1 Voltage Stability 19

2.3 Instability Concerns in Power System……..... 20

2.3.1 Voltage Instability 20

2.3.2 Phase Angle Instability 21

2.3.3 Dynamic Instability .....,,,,,..... 22

2.4 Modeling of Microgrids Inverters..... 23

CHAPTER 3

THEORETICAL FRAMEWORK & STATE SPACE ANALYSIS OF GRID FORMING INVERTER

3.1 Introduction 25

3.2 Modeling of Grid Forming Inverter 26

3.2.1 State space Model of Phase Lock Loop 28

3.2.2 State space Model of Droop Controller..... 30

3.2.3State Space Model of Voltage & Current Controller.....,,,,,…..... 33

3.2.4 State space Model of Time delay……..... 36

3.2.5 State space Model of LCL filter……..... 37

3.3 Model of Inverter..... 39

3.3.1 Model of Line..... 41

3.3.2 Model of Load……..... 41

3.4 Microgrid Model 41

3.5 Conclusion..... 43

CHAPTER 4

SMALL-SIGNAL STABILITY ANALYSIS OF VSIs IN A MICROGRID

4.1 Introduction 44

4.2 Eigenvalue and Sensitivity Analysis of Island Mode Microgrid Inverter 44

4.3 Testing Conditions and requirement of Distribution Energy Resources (DER)..... 49

4.4Implementing the System function in Matlab/Simulink..... 53

4.4.1 Case 1 Study and Results..... 56

4.4.1 Case 2 Study and Results..... 59

4.4.1 Case 3 Study and Results..... 55

4.4 Conclusions 60

CHAPTER 5

CONCLUSIONS AND FUTURE WORK……..……..…….57

5.1 Conclusions 61

5.2 Recommendations for future work 63

APPENDIX A

MATLAB/Simulink SCRIPTS 64

A.1 MATLAB main.m File 64

A.6 Reference 65

LIST OF FIGURES

Figure 1.1 (a) GFMI internal voltage source. 3

Figure 1.1 (b) GFLI Norton equivalent current source..... 3

Figure 1.2.1 Function diagram of grid-following inverters…...…….4

Figure 1.2.2 Function diagram of grid-forming inverters…….……...5

Figure 1.3.1 GFMI control methodologies…….…….7

Figure 1.4.1 A DG connected to the microgrid at point of common coupling (PCC)…..…..……..9

Figure 1.4 Inverter droop controller……..…….....11

Figure 2.4 Network Control System…….……..……14

Figure 2.5. Three different time delays of the system……..……..14

Figure 3.1 Block diagram of small signal state space model related……..……26

Figure 3.2 Model for the PLL…….……..……..26

Figure 3.3. Droop Power Controller…….…….…….28

Figure 3.4. Voltage and Current controller for grid feeding inverters……...32

Figure 3.5 Network Control System……..…….……35

Figure 3.6 Variable transformation for grid forming inverter…….……...40

Figure 4.1 Eigen vectors for VSI without Time Delay & PLL……..46

Figure 4.2 Eigen vectors for VSI with Time Delay & PLL @Time Delay 10ms.....46

Figure 4.3 Eigen vectors for VSI with Time Delay & PLL @Time Delay 100ms…….……...47

Figure 4.4 Eigen vectors for VSI with Time Delay & PLL @Time Delay 1s……...47

Figure 4.5. Actual Abnormal Voltage Requirements for Category III…….……..50

Figure 4.6 Actual Abnormal Frequency Requirements…….…….51

Figure 4.7 30kW Parallel GFM Inverters System……..…….53

Figure 4.8 Grid Forming Inverter control diagram……53

Figure 4.9 Active and Reactive Power @ Td=0, No Load Change……..……54

Figure 4.10 Output Voltage and Frequency at PCC @ Td=0, No Load Change……..…..……55

Figure 4.11 Active and Reactive Power @ Td=10ms, No Load Change……..55

Figure 4.12 Output Voltage and Frequency at PCC @ Td=10ms, No Load Change…….……56

Figure 4.13 Active and Reactive Power @ Td=100ms, No Load Change…….……56

Figure 4.14 Output Voltage and Frequency at PCC @ Td=100ms, No Load Change…….……..57

Figure 4.15 Active and Reactive Power at PCC @ Td=0ms, No Load Change……58

Figure 4.16 Output Voltage and Frequency at PCC @ Td=0ms, No Load Change……..……..58

Figure 4.17 Active and Reactive Power at PCC @ Td=0ms, Transient fault……...…...59

Figure 4.18 Output Voltage and Frequency at PCC @ Td=0ms, Transient fault……..60

Figure 4.19 Active and Reactive Power at PCC @ Td=0ms, Transient fault…….....60

Figure 4.20 Output Voltage and Frequency at PCC @ Td=0ms, Transient fault……..61

Figure 5.2.1 IEEE 9-Bus System 600MW……..……65

Figure 5.2.2 Case 1: Bus Voltage @ Time delay = 10us……..…….67

Figure 5.2.3 Case 1: Bus Frequency @ Time delay = 10us……..……..68

Figure 5.2.4 Case 1: LCL Network @ Time delay = 10us……...……68

Figure 5.2.5 Case 2: Bus Voltages @ Time delay = 0.1ms……69

Figure 5.2.6 Case 2: Bus Frequency @ Time delay = 0.1ms…….70

Figure 5.2.7 Case 2: LCL Network @ Time delay = 0.1ms……70

Figure 5.2.8 Case 3: Bus Voltages @ Time delay = 0.5ms……..71

Figure 5.2.9 Case 3: Bus Frequency @ Time delay = 0.5ms…….71

Figure 5.2.10 Case 3: LCL Network @ Time delay = 0.5ms…….72

Figure 5.2.11 Case 4: Bus Voltages @ Time delay > 0.5ms……73

Figure 5.2.12 Case 4: Bus Frequency @ Time delay > 0.5ms……73

Figure 5.2.13 Case 4: LCL Network @ Time delay > 0.5ms……..74

LIST OF TABLES

Table I Test System Parameters.....43

Table II Initial Conditions…….…….43

Table III. Eigen Vectors with Participation Factors w/o Time Delay & PLL…….……..44

Table VI. Eigen Vectors with Participation Factors with Time Delay & PLL…….…….45

Table V. IEEE 1547-2018 Frequency Requirement…….…….49

Table VI. IEEE 9-Bus System Parameter……..66

CHAPTER 1

INTRODUCTION

1.1 Motivation for this Research Work

As growing numbers of inverter-based resources (IBRs) are deployed—including wind turbines, solar photovoltaic (PV) arrays, and batteries—their role on the grid is changing, and the grid services needed from them have evolved. Inverters in service today are predominantly "grid following" (GFL) [3]. IBRs differ from conventional synchronous generators in that they are not physically synchronized to the grid but are interfaced through power electronics. As a result, IBRs do not inherently respond to disturbances on the grid, as synchronous machines do. This poses both challenges and opportunities to a grid that was historically designed around synchronous generators. In addition, two decades ago when IBRs were scarce, they were allowed, or even required, to cease operation during disturbances on the grid. But gradually, as shares of these resources began to increase, such behaviour exacerbated the severity of system disturbances. Consequently, interconnection standards for IBRs evolved to ensure that they can ride through certain types of frequency and voltage disturbances without disconnection and can also contribute to fault recovery. Increasing levels of IBRs have also led to the decommitment and, in some cases, retirement of synchronous generators that were providing system services to support voltage and frequency, either inherently, mandatorily, or through market products. In order to maintain grid stability and reliability, IBRs need to provide some of these services such as frequency and voltage support. Requirements of capability for these services are now being included in interconnection standards, and the rules for their procurement and deployment can be implemented as mandatory interconnection requirements or market products. The inverters used in IBRs are generally designed to follow the grid voltages and inject current into the existing

voltage. Therefore, they are known as grid following inverters (GFLIs). The common technique used to synchronize with the grid voltage is the use of a phase-locked loop (PLL). This grid following behaviour resembles a current source. All of the currently installed IBRs fall into this category, and thus, voltage source behaviour is not intrinsically present in IBRs. Moreover, IBRs are not designed with sufficiently large energy storage to emulate inertial response. The over-current ratings of the power electronic switching devices used in inverters are also low compared to synchronous generators. Therefore, IBRs are considered as non-synchronous generation sources. This ideal voltage source behaviour and high inertia are the essential features for maintaining a stable power grid. The major challenge with the increased penetration of non-synchronous generation sources in power systems is the voltage and frequency regulation [2]. New voltage stability concerns are created due to the following:

- the varying number of online voltage regulators with high gains
- differences in IBR responses
- potential interaction between IBRs and other dynamic devices.

Microgrids, which can operate in the grid-connected mode as well as in the islanded mode, emerged as a platform for integrating IBRs. The concept of grid forming inverters (GFMIs) originated from this need. Furthermore, the need for emulating the features of the synchronous generators emerged as the concept of microgrids evolved. The controls of GFL inverters rely on continuous measurements of the grid voltage (the phase and magnitude) and react by rapidly and tightly governing the output current. However, in areas of low system strength, the voltage becomes more sensitive to current injection. This results in an inaccurate voltage measurement and an incorrect reaction from the GFL controls, leading to possible instability. The transient stability of power systems will be reduced when the penetration of grid-following inverters increases due

to the reduced inertia of synchronous generators [5]. In contrast, grid-forming inverters (GFMIs) control voltage and frequency instead of currents. They behave as voltage sources behind reactance. The capability of grid-forming inverters (GFMIs) to maintain the voltage and frequency stability has been extensively studied in microgrid research [6].

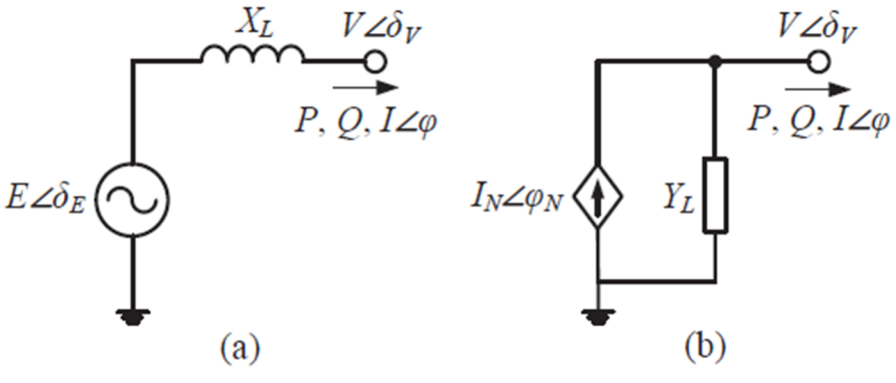

Figure 1.1 (a) GFMI internal voltage source. (b) GFLI Norton equivalent current source.

1.2 Why Grid Forming Inverters (GFM)?

A grid-forming inverter fundamentally behaves as a voltage source behind a coupling reactance XL, which controls both the voltage magnitude E and the angular frequency ω, as shown in Fig. 1. The coupling reactance, XL, plays a critical role in controller design. By properly sizing XL (e.g., between 0.05 and 0.15 pu on an inverter rating base), the active power P and the reactive power Q are decoupled. As shown in (1)–(3), P is approximately linear with the phase angle difference δP, and Q is approximately linear with the internal voltage magnitude E. This decoupling reduces the controller design complexity [3] Grid forming inverters are traditionally used to inject active power into the PCC at unity power factor. As mentioned in the introduction, GFM are expected to perform as synchronous generators, and thus, it is essential to emulate the key features of synchronous generators, such as the ability to supply constant/committed power to the grid, inertial response, and fault current behaviour as much as possible. Some form of

energy storage is required to maintain committed power delivery, irrespective of the changes in the wind or solar power input. Similarly, the inertial response requires energy storage, at least for the duration of the required response. Therefore, the need for energy storage is another major difference between GFLIs and GFMIs.

$$\delta_P = \delta_E - \delta_V \tag{1.1}$$

$$P = \frac{EV}{X_L} sin\delta_P \approx \frac{EV}{X_L}\delta_P \tag{1.2}$$

$$Q = \frac{E^2 - EVcos\delta_P}{X_L} \approx \frac{E(E-V)}{X_L} \tag{1.3}$$

1.3 Grid Interaction capabilities of GFL and GFM

The primary objective of supplying active and reactive power to the grid is common for all IBRs. However, depending on the interaction with the grid, controller implementation and response to the changes in the grid, they can be classified into two main groups, namely: GFLIs and GFMIs, as shown figure 1.2.1.

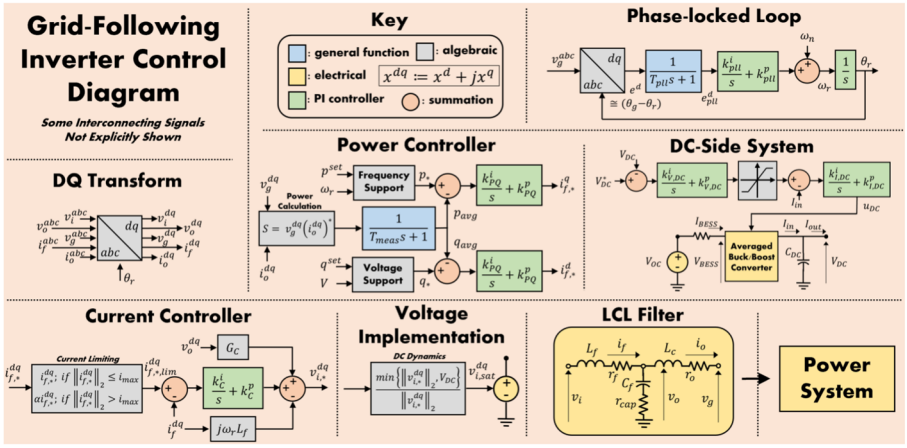

Figure 1.2.1 Function diagram of grid-following inverters.[2]

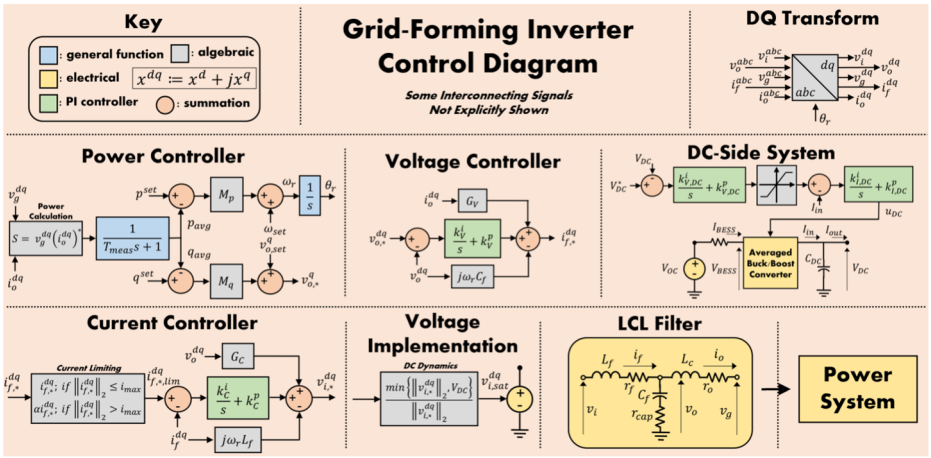

Figure 1.2.2 Function diagram of grid-forming inverters.[2]

In Fig. 1 (a). As mentioned in the previous sections, applications of GFLIs are primarily focused on active power injection into the grid with maximum power point tracking (MPPT). Therefore, the reactive power supply is minimum and often close to zero. Such inverters are known as grid-feeding inverters (GFD). From a revenue point of view, it is more attractive to run IBRs as GFD. Nevertheless, voltage and frequency regulation become challenging as the number of GFD increases. The fundamental difference in grid interaction of GFMIs come from the way active and reactive power delivery to the grid is controlled. As mentioned above, the primary objective of GFL is to inject active power to the grid, and supporting the grid is the secondary objective. In contrast, in GFM, the primary objective is regulating the voltage and frequency of the grid. Therefore, active, and reactive power references are continuously varied in GFM to achieve this objective. There is evidence that grid-forming inverters can play a constructive role in improving the frequency dynamics and stability of inverter-dominated power systems [4]. From the control point of view, the behaviour of a GFL can be approximated to a controlled current source with a high impedance in parallel, as shown in Fig. 1.1 (b). A GFL measures the voltage at the PCC (V_{PCC}) and derives the phase angle of the V_{PCC} via a PLL. Then, the terminal voltage is varied such that the desired direct- and quadrature- (d-q) line currents are achieved. The active and reactive

power support from a GFL is achieved by controlling the injected d and q currents, respectively. In contrast to a GFL, a GFM can be approximated to a voltage source with a low series impedance, as shown in Fig. 1.1 (a). Contrary to GFLIs, GFMIs do not measure the V_{PCC} for synchronization purposes and rather form the V_{PCC} to regulate their power output. Another major difference between the GFLI and GFMI control is that a GFMI can operate/supply the local loads in the absence of grid connection by establishing its own reference voltage and frequency. In a steady-state operating condition, depending on the control topology, power set-points and grid conditions, both GFLIs and GFMIs can inject active and reactive power to the grid. However, one of the main differences in performance between GFLIs and GFMIs lies in the reaction of each of these inverters to a grid disturbance in weak grids. Active and reactive power support during a disturbance, which is also known as virtual or emulated inertia support, can be implemented in both GFLIs and GFMIs depending on the source type. In the case of a GFLI, the disturbance is measured through voltage and current measurements, and appropriate control actions are taken for grid support functionality. As the internal voltage phasor of the GFMI is not affected at the beginning of the disturbance, an instantaneous response of power can be achieved depending on how fast the grid angle changes. Even though the reaction of a GFMI is much faster compared to its GFLI counterpart, concerns on current limitations and stability with rapid responses need to be addressed. Another difference in the performance between GFMI and GFLI control is the small-signal stability behaviour under weak grid conditions. With GFLIs relying on grid voltage and angle measurements to remain synchronized to the grid, the stability margin can be greatly reduced with sudden changes in the measured grid signals. This problem is greatly reduced in GFMIs with the possibility of self-synchronization using phase lock loops and the absence of dependency on

grid signals for synchronous operation. Detailed discussions on the control methodology, performance, and limitations of the GFMIs are provided in the following sections.

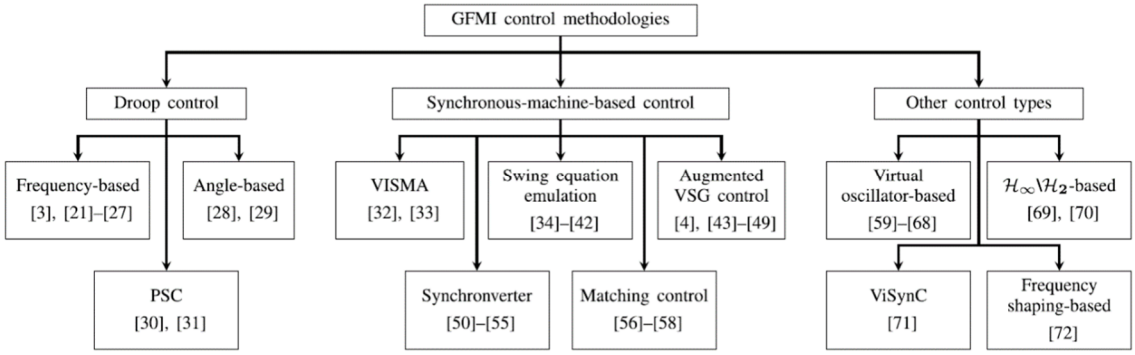

Figure 1.3.1 GFMI control methodologies [1]

1.4 Grid Forming Inverter (GFM) Functions

Droop control is a well-established technique to control an autonomous grid. In fact, the Active Power/ Frequency (P/F) and Reactive Power/Voltage (Q/V) droop control mimics the operation of synchronous generators in a transmission system. With the droop control technique, PLL are not required to achieve system-wide synchronization because all inverters reach the same frequency. In addition, power sharing among each inverter can be achieved since each inverter gives power in proportion to its capacity. The droop P/F is set to a percentage meaning that microgrid frequency is allowed to variations around 60 Hz. This is done, when the inverter produces no active power to decrease its frequency and produces its nominal active power to increase its frequency. The droop Q/V is set to a droop percentage meaning that the microgrid voltage at the PCC bus is allowed to variation of its set V_{rms} voltage, it the penetration is too high, the inverter produces its full inductive power. If the V_{rms} is too low, the inverter produces its full capacitive power to increase. Based on the frequency value given by the Droop control, the measurement subsystem computes the active and reactive power generated by the inverter. It also computes the d-q components of the three-phase voltages and currents at the microgrid PCC bus. From the figure

1.2.2, the method of control for the grid forming inverter is the angle-base drooped. High gain angle droop control ensures proper load sharing, especially under weak system conditions. However, it has a negative impact on overall stability. Frequency-domain modeling, eigenvalue analysis, and time-domain simulations are used to demonstrate this conflict [7]. The control law for this method is presented as;

$$\omega = \omega_{rated} - m_P(P - P_0) \tag{1.4}$$

$$V = V_{rated} - m_Q(Q - Q_0) \tag{1.5}$$

where ω and V are the phase-angle and magnitude of the terminal voltage, w_{rated} and V_{rated} are the phase-angle and magnitude of the terminal voltage when the inverter is outputting rated active power (P_0) and rated reactive power (Q_0), and M_P and M_Q are the corresponding active power and reactive power droop coefficients, respectively. The M_P and M_Q values are chosen based on the voltage regulation and proportional load sharing requirements.

1.4.1 Droop Controller

The objective of the droop controllers is to maintain the overall response of the system. Droop control concept originates from the governor action that enables the parallel operation of multiple synchronous generators. A droop controller involves several stages of processing, particularly output power calculation and updating the voltage command setpoint. These stages contribute to a time delay defined in [12] as the droop response time (DR time), which can vary between multiple DG units because of different designs and controller implementations.

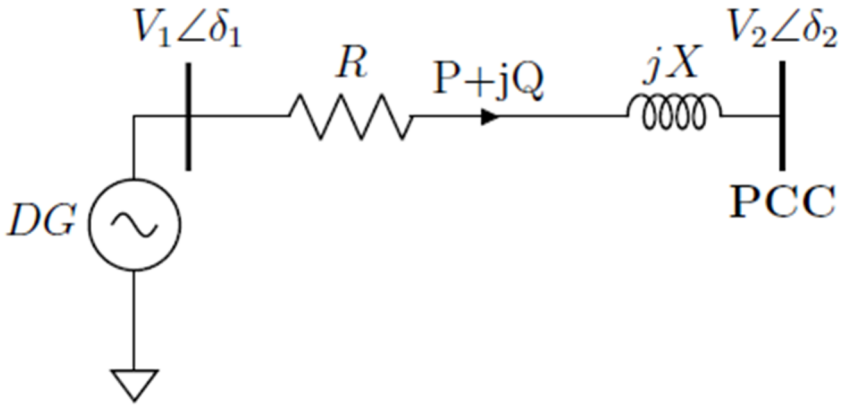

Figure 1.4.1 A DG connected to the microgrid at point of common coupling (PCC).

The droop controlled GFMIs can operate with multiple GFMIs and GFLIs in both grid-connected mode and standalone mode. The droop controlled GFMIs can operate with multiple GFMIs and GFLIs in both grid-connected mode and standalone mode.

Consider a source connected to the point of common coupling (PCC) through a line, with impedance Z=R+jX Ω, as shown in Fig 1.4. Where the source can be a DG or a synchronous generator (SG), here it is assumed to be a DG. V1∠δ1 and V2∠δ2 are voltages at DG terminal and at PCC, respectively. Real (P) and reactive power (Q) flow from DG to the PCC is given by:

$$P = \frac{R\left(V_1^2 - V_1V_2\cos(\delta_1-\delta_2)\right)+X(V_1V_2\sin(\delta_1-\delta_2))}{R^2+X^2} \tag{1.6}$$

$$Q = \frac{-R(V_1V_2\cos(\delta_1-\delta_2))+X\left(V_1^2 - V_1V_2\sin(\delta_1-\delta_2)\right)}{R^2+X^2} \tag{1.7}$$

It can be seen from (1.1) and (1.2) that both P and Q are dependent upon voltage and power angle, and impedance of the line. In a droop control P and Q are regulated by regulating voltage (V1) and δ1 of DG. Hence, in order to control P and Q it is important to find the sensitivity of P and Q to V and δ1. Sensitivity of P and Q to V1 and δ1 can be given by:

$$\frac{\partial P}{\partial \delta_1} = \frac{R(V_1V_2\sin(\delta_1-\delta_2))+X(V_1V_2\cos(\delta_1-\delta_2))}{R^2+X^2} \tag{1.8}$$

$$\frac{\partial P}{\partial V_1} = \frac{R(2V_1 - V_2\cos(\delta_1 - \delta_2)) + X(V_2\sin(\delta_1 - \delta_2))}{R^2 + X^2} \tag{1.9}$$

$$\frac{\partial Q}{\partial \delta_1} = \frac{-R(V_1V_2\cos(\delta_1 - \delta_2)) + X(V_1V_2\sin(\delta_1 - \delta_2))}{R^2 + X^2} \tag{1.10}$$

$$\frac{\partial P}{\partial \delta_1} = \frac{-R(V_2\sin(\delta_1 - \delta_2)) + X(2V_1 - V_2\cos(\delta_1 - \delta_2))}{R^2 + X^2} \tag{1.11}$$

It can be observed from (1.8)-(1.11) that any change in δ1 will result in a change in P and Q generated by DG. Similarly, any change in V1 will affect P and Q both. One of the reasons for this coupling is it is caused by feeder impedance (R and X) or R/X ratio, as we will see that for inductive or resistive feeders this coupling vanishes. The analysed the sensitivity for different R/X ratios of lines. Since, for a transmission system, R/X ratio of the line is smaller than R/X ratio of the line in the distribution system. Therefore, the sensitivity of P and Q will differ for both systems. This will be discuss in chapter 3.

The control strategies that coordinate the IBRs either utilize high bandwidth communication channels or depend solely on local measurements. The droop control only depends on the local measurements and does not require any inter-inverter communication. Thus, the implementation of droop controllers is hassle-free, and redundancy is easily achieved [3]. further improve the transient response of the classic droop control (proportional control), in [3], derivative and integral terms are incorporated into the droop controller of the active power path. In contrast, only a derivative part is incorporated into the droop control in the reactive power path. Incorporating derivative and integral terms into the droop controller overcomes the issues such as voltage

deterioration with large droop gains, limited power sharing accuracy, large transient circulating currents, and stability issues that are common in droop-controlled inverters.

The P-f droop control and Q-V droop control enable multiple grid-forming inverters to work together in a microgrid. The P-f droop control balances active power between inverters, and the Q-V droop control mitigates circulating reactive power between inverters. P_f, Q_f and V_{magf} are filtered values of active power, reactive power, and voltage magnitude, respectively. Conventionally, the real power–frequency droop control and the reactive power–voltage droop are adopted as the de-centralized control strategies in these DICs for the autonomous power sharing operations [8].

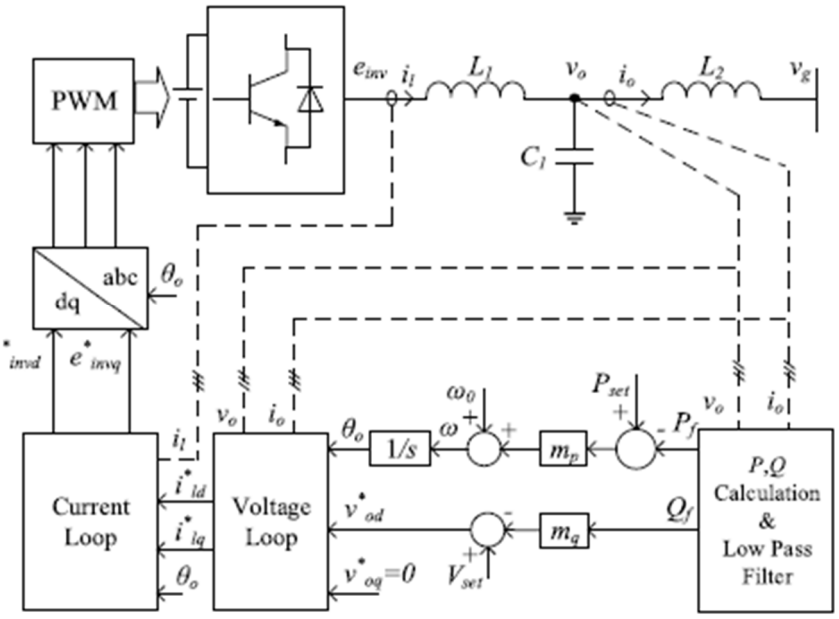

Figure 1.4 Inverter droop controller.

1.4.2 Active Power-Frequency Droop control

Due to the replacement of synchronous generators, grid operators are currently demanding to control grid-connected inverters in grid–forming mode to make them participate in the maintenance of the grid. To carry this out, the traditional droop controls based on the active and

reactive powers are usually adopted, achieving a satisfactory performance in normal operation. Nevertheless, the power-frequency (P-ω) droop may become transiently unstable under voltage dips. This is because of the modification of the active power response caused by the inverter current limitation together with the voltage reduction. P-f droop control method is suitable for networks with low X/R ratios.

1.4.3 Reactive Power -Voltage Droop control

A reactive power voltage (Q-V) droop control is used to control point of common coupling (PCC) voltage magnitude while an active power frequency (P-f) droop control is used to control the frequency of the system in islanded mode [6]. Q-V droop control method is suitable for networks with high X/R ratios.

1.4.4 Phase Lock Loop

In inverter-dominated power systems, the grid cannot be modelled as a stiff voltage source with constant frequency. Most existing grid-connected inverters operate as grid-following sources in which they measure the frequency at the inverter terminals using a phase-locked loop (PLL). Recent studies have indicated that the PLL controls can result in instability in weak systems. Although, this isn't a key component in designing a GFM, it plays a role in behaving as synchronous tool that regulates the internal frequency and voltage to the grid [24]. It acts as a 'synchronizing torque' as like the synchronous generator. This helps in modelling the GFM.

1.4.5 Voltage controller

Reference voltage V_{ref} given by the Droop Control is fed to the Voltage controller. This controller is a simple PI controller. The regulators process the measured d-q voltages and reference voltage V_{ref} to generate the reference currents I_{d_ref} and the I_{q_ref}.

1.4.6 Current controller

The I_{d_ref} and the I_{q_ref} reference currents are fed to the Current controller. This controller is a simple PI controller. The regulators process the measured and reference currents to produce the required d-q voltages ($V_d V_{q\_conv}$) for the inverter. Note that the regulators dynamics benefits from a feed-forward calculation.

1.4.7 Time Delay Model

It is well known that time delay degrades the dynamic performance and even violates the stability of a control system. The study of time-delay systems has received wide interests [13],[14]. Time delay modelling is used to emulate the communication and response delay within the controllers and filters used in the grid forming inverter. To elaborate further, internal construction as described in the previous chapters are considered being ideal components. However, we know this isn't the case. Each of the controllers described earlier has a form of delay, which was investigated in [11,12]. In order to avoid the difficulties in directly solving the transcendental characteristic equation of each device, a simple model of delay-dependent stability, $\frac{1}{\tau_s+1}$ criteria have been proposed to analyse the stability of a power system against time delay. To discover the trade-off between the robustness of protocol to the channel's time delay and its performance.[15] Figure 2.4 describes the concept of delay between controllers, sensor and actuator within a system. Our goal and objectives are to combine theses delay into a single unit that models the total delay within a power system network, and analysis its affect on the internal stability of the grid forming inverter.

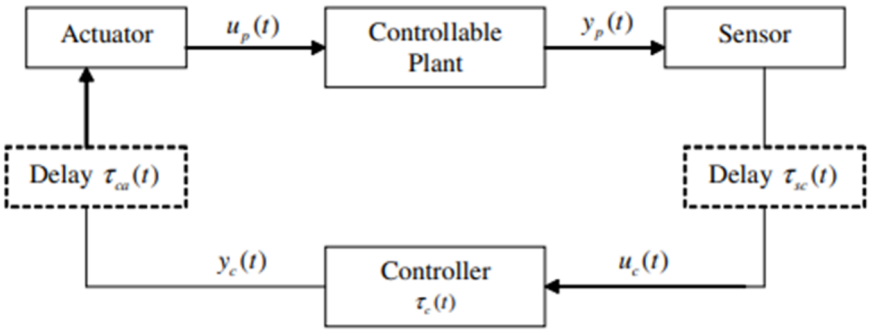

Figure 2.4 Network Control System

For a fully connected system, the number of connections equals to $n(n-1)$. The system can reach consensus within one step. However, for practical power systems, the iteration matrix is usually a sparse matrix, and so it takes time to reach an agreement, which results in a time delay. This time interval is called agreement time delay. There are also two other time delays, namely the channel's time delay and the controller's time delay. All these three different kinds of delay are shown in Figure 1.5.

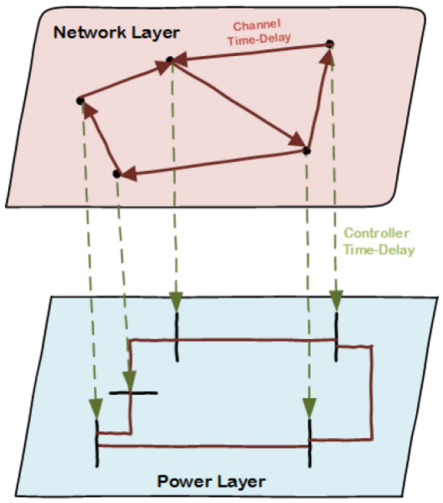

Figure 2.5. Three different time delays of the system.

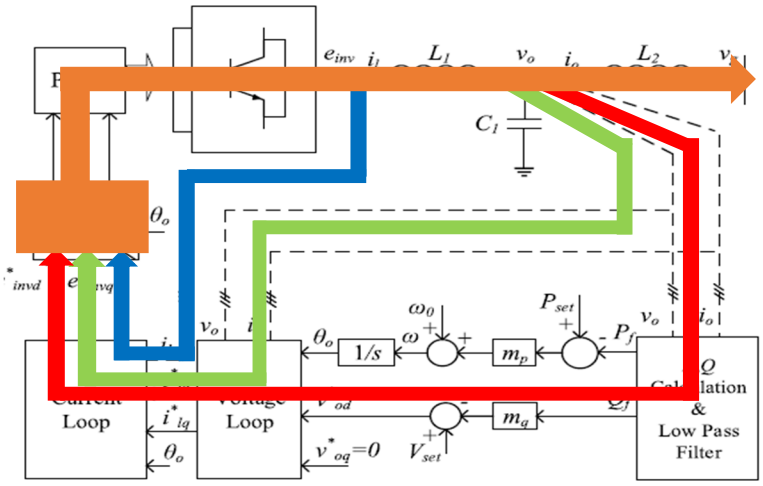

Figure 2.6 Time Delay topology of grid forming inverter.

Figure 2.6, we see a multi-loop inverter with various controllers and strategies. It is known in a few papers, that these loops have some delay aspects that are not modeled in a microgrid system. Not to mention the other types of sensors and filters. Which has some impact on the internal stability of the grid-forming inverter. The first level is the inner loop, which includes the voltage control loop and an inner current control loop. (The Green and Blue lines respectively). This control strategy is known as cascade control. Control is responsible for instantaneous tracking of the system's nominal voltage and power quality issues at this level. At the second level (the red line) is the primary control with strategies related to system stability, voltage and frequency stability, and power sharing in the load's connection. Within these loops, are controllers, sensors, filters, and other power electronics devices, which have some form of delay that impacts the system's stability. My goal is to derive this state space equation of the timescale delay in the grid-forming inverter at the point these loops meet and be received by the inverter (The Orange Line). Where we know that the response across any element in the circuit is the sum of the responses obtained from each loop considered separately.

1.5 Objective of the Thesis

Since the study of a microgrid is still an evolving topic it has been observed that some elements such as droop controllers, voltage controller, current controller, Phase Lock Loop control are not modelled in detail for the stability study of the system. It was shown in [14] how detailed modeling time delay within a controller can help in understanding the cause of high frequencies in the system following a disturbance.

The main objective of this thesis is to model and evaluate the impact of various time delay of Grid Forming inverters, particularly those equipped with droop control functions and testing their ride-through capabilities under transient faults in a microgrid system. As IBRs replace synchronous generators and reduce system strength, the transient stability concern may be replaced by a need to maintain adequate voltage and angular stability across the grid. This will be done in the following 4 steps:

1. Selecting the proper software package to address modelling of the grid forming inverter, microgrids system and stability analysis. As well as testing the microgrid inverter robustness under fault conditions. Modelling a distributed generation seems redundant and does not achieve the objective task. However, there are examples that will be implemented to test various cases. Traditional analysis tools like MATLAB/ Simulink can conduct various control analysis techniques so it must be ensured that a capable software package is selected to accommodate for this.

2. Develop a working state space model of the microgrid grid forming inverter with their relative time delay sequences for each stage of the inverter. Combine these state equations to generate an overall state space equation for the grid forming inverter.

3. Applying Root locus methods, Eigen values and discovering the participating factors in the microgrid inverter with time delay & Phase Lock Loop.

4. Design a working model in MATLAB/Simulink to Validate the data found.

5. Simulating the frequency response to transient faults in MATLAB/Simulink. Selecting various conditions, such as time delay, sample time and droop percentages.

1.6 Organization of the Thesis

The overall structure and layout for thesis will cover the motivation behind grid forming inverter. The desired control scheme (i.e., droop control) used will be investigated along with case studies. Theoretical behind the analysis of Grid forming inverter will be presented.

- Chapter 2 is a Literature survey; this chapter presents a survey concerning stability in a power system and microgrid modeling and controls. Supporting that a delay exist within each device in the controller.
- Chapter 3 introduced the theoretical behind the analysis of Grid forming inverter. The state space model described in [9] will comprise the complete design process for the selected case studies and distribution system with a modelled time delay to emulate the inertia effect of a typical synchronous generator (SG). Modelling of the time delay will be as describes in [10,12]. This state equation will be defined and transpose into MATLAB. Defining state variables and participating factors.
- Chapter 4, using MATLAB/Simulink the simulation process, stability analysis and participation factors for the Grid Forming inverter functions for selected IBR penetration scenarios for both case studies will be presented.

- Chapter 5 concluded the finding and analysis of the effects of time delay in the system. Along with a state space model development for future studies. This chapter also includes the future work which can be carried out based on the work presented here.

CHAPTER 2

LITERATURE SURVEY

2.1 Introduction

As discussed in the previous chapter, as power systems around the world integrate greater amounts of wind and solar photovoltaic power, periods of very high instantaneous power shares of inverters, the primary interfacing technology for these generation sources, are complicating system stability and control. The contemporary, primary mode of inverter operation, grid-following, which explicitly assumes the presence of a local, stable voltage waveform, yields operational inadequacy at high instantaneous power shares potentially leading to instability due to the low-inertia conditions, as well as the correlated reduced voltage forming capacity on the respective system. The benefit of a single grid-forming device over its grid-following counterpart is significant, both in terms frequency deviation and voltage stability. Further, the superiority of the Droop controller and the associated secondary power sharing control over both grid-following and linear droop grid-forming technologies is displayed, with improved nadir and rate of change of frequency over the linear droop control. Moreover, we must understand the different types of stabilities that can affect the power system and correlate that knowledge to set a benchmark to determine the robust nature of a grid forming inverter.

In this chapter, a literature survey related to the problem investigated in this research is presented. The survey is organized as follows; In section 2.2 and 2.3, works related to the stability concerns in grid forming inverter and types of instability in a power system are presented respectively. Finally, in section 2.4, surveys on microgrid modeling are covered.

2.2 Stability Concerns in Grid Forming Inverter

In this part, a survey of studies of the stability concerns with Inverter Base resources within the power system. As well the contributing factors that makes the grid unstable. Examples and situations will be explained and discussed.

2.2.1 Frequency Stability

In a power system, frequency is a measure of the balance of MW generation and MW load. When MW generation and MW load are exactly in balance, the frequency is at the normal level of 60 Hz. When load exceeds generation, the frequency goes down. The rate of decline depends on the inertia of the generators within the system. [Under normal conditions, there are slight changes of frequency when load suddenly increases or generation trips off-line which results in a slight (generally in the hundreds of a Hz) reduction in frequency until the aggregate generation in the system can be increased to meet the new load condition. If there is a large negative unbalance between MW load and MW generation, the frequency will go down.

2.2.2 Voltage Stability

Voltage in a power system is a measure of the balance of MVAr load and MVAr capability within the system. If that reactive support is not available, the voltage will go down. The impact of reduced voltage on load depends on the nature of the load. For resistive load, the load current will decrease and help limit the need for local reactive support. Motor loads are essentially constant kVA devices. The lower the voltage, the more current they draw—increasing the need for local reactive support. Power systems loads consist of both resistive loads as well as reactive motor loads. Reactive power system support can only come from two sources: shunt capacitors and generators/synchronous condensers.

2.3 Instability Concerns in Power System

The grid-forming inverter should be able to generate an AC voltage with a given amplitude and frequency at Point of Common Coupling (PCC) like a (Synchronous Generator) SGs. Unlike inverters, SGs possess inertias and damping factors in terms of their structural properties, which introduce a slow dynamic to the frequency that is a result of rotational speed. The primary control also allows inverters to synchronize to the grid without detecting the grid-phase and to share power with other generators. The understanding of power system stability has taken on renewed importance because it has played an important role in recent blackouts and power system events investigated by NERC. The are four basic types of power system instability: Voltage instability Steady-state instability, Transient instability, and Dynamic instability.

2.3.1 Voltage instability

Power system voltage stability is characterized as being capable of maintaining load voltage magnitudes within specified operating limits under steady state conditions. In the case of the 2003 East Coast blackout [1], three key transmission lines were lost in succession due to tree contacts. The voltage at the load center was reduced before the system operators could take effective corrective action. Effective operator action was inhibited by the lack of data from key transmission system substations due to a computer problem at the system operating center. In the case of the 2003 East Coast blackout, voltage decay was relatively slow and there was time for system operator intervention to address the voltage decay problem. During system low voltage conditions, distance relays are susceptible to false operation on load. While the ohmic characteristic of a distance relay is independent of voltage, the load is not a constant impedance. The apparent impedance presented to a distance relay as the load voltage varies will depend on the voltage characteristics of the load.

2.3.2 Phase Angle instability

When the voltage phase angle between remote generators and local generators (θg – θs in Fig. 4) becomes too large, phase angle instability can occur. In many cases, this event happens in conjunction with the voltage collapse scenario described above. There are two types of phase angle instability. As previously discussed in this paper, there are two types of phase angle instability -- SteadyState and transient instability. Both these instability conditions impact transmission as well as generator protection and manifests them as power system swings as the phase angle separate. Interestingly, the industry practice is to block tripping for swings on the transmission system using out-of-step blocking logic and to trip on generators if the power swing passes through the generator or generator step-up transformer.

i. Steady-State Instability: Steady-state instability occurs when there are too few transmission lines to transport power from the generating source to the local load center. Loss of transmission lines into the load center can result in voltage collapse as described previously, but it can also result in steady-state phase angle instability. Many large power plants have very few transmission lines which connect them to the system. As a result, there have been cases where the proper tripping of transmission lines exiting the power plant have left the generator connected with too high impedance connect to the system. Where this condition is credible, SPS schemes have to be put in service to trip the generator to address this instability.

ii. Transient Instability: Voltage phase angle instability can also occur due to slow-clearing transmission system faults. This type of instability is called transient instability. Transient instability occurs when a fault on the transmission system near the generating plant is not

cleared rapidly enough to avoid a prolonged unbalance between mechanical and electrical output of the generator. A fault-induced transient instability has not been the cause of any major system blackout in recent years. However, generators need to be protected from damage that can result when transmission system protection is slow to operate.

2.3.3 Dynamic instability

Dynamic Instability occurs when a fast-acting generator AVR control amplifies rather than damps some small low frequency oscillations that can occur in a power system. This problem has been most often associated with the western region of the U.S. It can, however, occur anywhere the load is remote from the generation. While fast excitation systems are important to improve transient stability as discussed above, a fast-responding excitation system can also contribute a significant amount of negative damping. This reduces the natural damping torque of the system, causing undamped megawatt oscillations after a disturbance such as a system fault. It can occur if the generator is interconnected to a weak system and loads are far from the generating plant. Small signal stability is defined as the ability of the power system to remain stable in the presence of small disturbances most often caused by remote faults. If sufficient damping torque does not exist, the result can be generator rotor angle oscillations of increasing amplitude. When these megawatt oscillations grow, the generator can eventually be driven unstable, lose synchronism and slip a pole.

Power system stability has taken on an important role in recent blackouts and power system event investigations conducted by NERC. How the various types of instability relate to protection is important to understand so stability can be properly considered when a more robust voltage source inverter in a power system. Recall in the introduction of this thesis, that the fundamental idea for

a grid forming inverter is to act as a voltage source and to emulate the function of a synchronous generator.

2.4 Modeling of Microgrids Inverters

In order to develop a control strategy for a microgrid, an appropriate state-space model is needed. There are few works focusing on inverter-based microgrid modeling [17, 18, and 19]. In [19], Pogaku et.al. presented a modeling and analysis of autonomous operation of inverter-based microgrids. The model captures details of the inverter's control loops but not the switching actions or delays. This paper has modelled only Voltage Source Inverters (VSI), and the time & phase delay impact are not considered. Furthermore, the effect of changing nominal frequency and voltage set points in state space modeling are not considered, which prevents implementing a phase lock loop system to act as a form of stabilizing, synchronizing and monitoring the grid. In [11], an approached to approximate and model the time delay has been presented. This paper discusses the theory behind pade' approximation and their respective representation to perform a time estimate or approximation. There are a few works that focus on time delays within different controller devices [14,15,16]. By their respective work, we can summarize that there is a form of delay, that is not being taken into consideration in the controllers and components that are used in implementing a voltage source inverter. From [16], this paper discusses consensus problems for networks of dynamic agents with fixed and switching topologies. This looks at the directed networks with fixed topology; directed networks with switching topology and undirected networks with communication time-delays and fixed topology. This provides evidence that there is a form of delay in the controller design of the grid forming inverter, which was lacking in [19].

CHAPTER 3

THEORETICAL FRAMEWORK AND STATE SPACE MODELING OF GRID FORMING INVERTER

3.1 Introduction

Distribution system infrastructure has changed a lot in the past few years. With the introduction of renewable sources such as wind, photovoltaics, fuel cells, etc., it is possible to operate a small part of the distribution system on its own; such a small set of loads and sources is called as microgrid. In a grid-connected microgrid, renewable sources help in fulfilling the real power demand of the grid. But when disconnected from the grid due to any reason, such as fault, the renewable sources play a vital role in system dynamics and can maintain voltage and frequency within acceptable limits, and such a microgrid is called an islanded Microgrid.

The objective of this chapter is to present the theoretical framework for evaluating the island operation of an inverter-based micro using droop control technique in GFMIs. Deriving their respective state equations. Firstly, referring to [19], this reference is suitable due to their extensive research and validity on this topic. Hence, this chapter begins with selecting the appropriate software tools for considering the time variation of GFMIs in a microgrid.

A small signal state space model of the microgrid is needed to analyse the stability of the microgrid under small disturbances. A complete model of a microgrid is presented in [18], where every system element is modelled in its state-space form, and then a system matrix is formed using individual matrices.

In practice, a DG is connected through a transformer instead of a coupling inductance. Transformers can be connected to the source side for changing voltage levels and for electrical isolation; they can also be connected to the load side to serve load at their respective voltage

rating and for serving load connected in different configurations than that of the distribution system etc. Dynamic equations of delta-grounded wye transformer connecting the DG to the bus are presented in [16], but modeling of other transformers is not present in any literature.

It is important to model each electrical element that could be present in a microgrid so that an accurate study can be performed regarding the stability of the microgrid. An attempt has been made to model the transformer's state-space equation would be prevalent so that the transformer model can be used for more accurate small signal stability analysis. For simplicity, we choose to ignore the isolation transformer model reference and kept the simple LCL filter configuration, for this is not the scope of this thesis. However, this would be a strong consideration in future works in Chapter 6.

3.2 Modeling of Grid Forming Inverter

VSI inverters are mostly used to connect distributed generators to the network. Figure 3.3 shows the block diagram of a VSI inverter connected to a microgrid. It has a power electronic section including a three-leg inverter, an output filter and a coupling inductor. Assuming an ideal source from the DG side, the DC bus dynamics can be neglected. There is also a control section comprised of three parts: (1) a power control loop that sets the voltage magnitude and frequency of the fundamental component of the inverter output voltage according to the defined droop characteristics related to the real and reactive powers. (2) The voltage and (3) current controllers. In many papers, the dynamic of the second and third controllers are eliminated for simplification purposes [10]; however, in this work, the detail of these parts are considered in order to have a more accurate model. A state space model is presented for all of the subsystems: control loops, output filter and coupling inductor. The model is constructed in a rotational reference frame set by the power controller of the individual inverter. The small-signal flow among the modules is

shown in Figure 3.2. Network dynamics are generally neglected in the small-signal modeling of conventional power systems due to the small time constant of the network compared to the rotating machines and their controllers. By contrast, microgrids have inverter-based generating units whose response times are very small so network dynamics can influence the system stability.

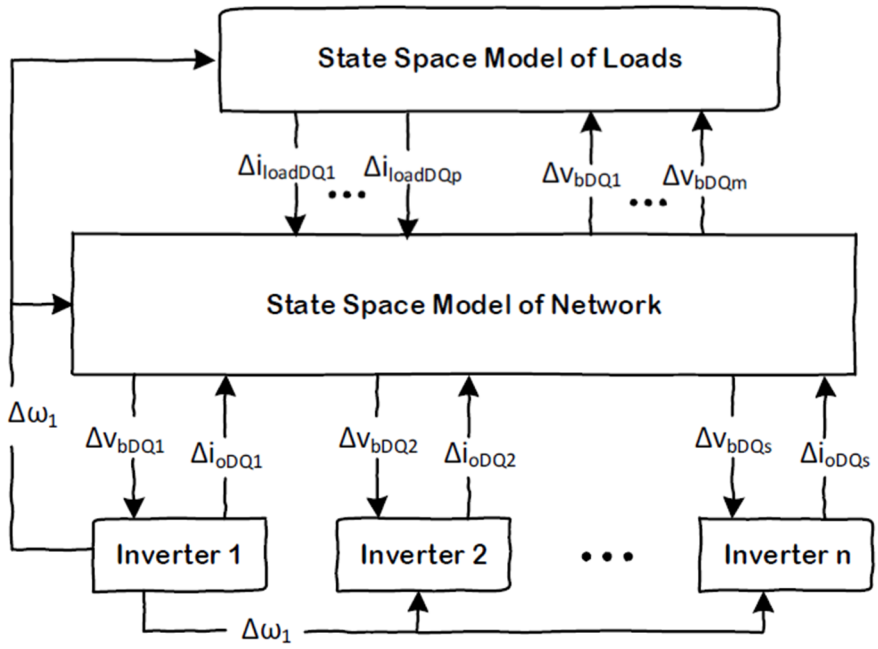

Figure 3.1 Block diagram of small signal state space model related to the microgrid component.

3.2.1 State Space Model of Phase Lock Loop

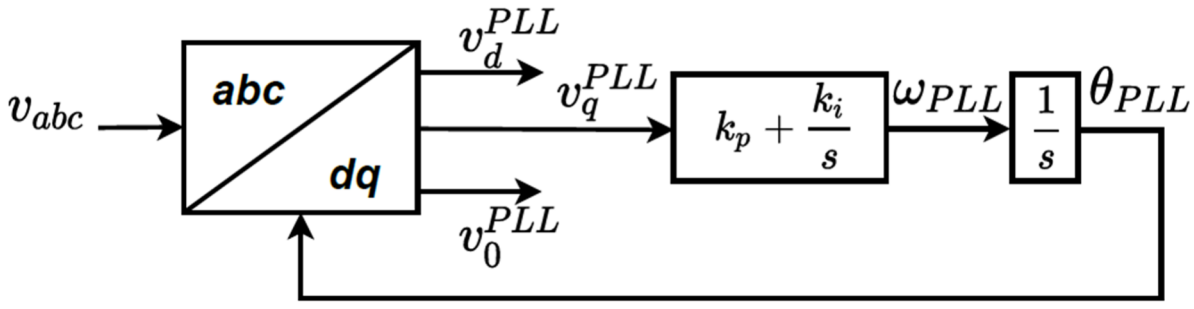

Figure 3.2 Model for the PLL

The PLL system indicated in fig. 2. For the grid forming inverter require a PLL unit to track voltage and frequency at the point of common coupling (PCC) as shown. Park transformation to convert from grid abc-voltages to dq0 is given as:

$$f_{dq0} = P(\theta) f_{abc} \tag{3.1}$$

Where,

$$P(\theta) = \sqrt{\frac{2}{3}} \begin{bmatrix} cos\theta & \cos\left(\theta - \frac{2\pi}{3}\right) & \cos\left(\theta + \frac{2\pi}{3}\right) \\ -sin\theta & -\sin\left(\theta - \frac{2\pi}{3}\right) & -\sin\left(\theta + \frac{2\pi}{3}\right) \\ \frac{1}{\sqrt{2}} & \frac{1}{\sqrt{2}} & \frac{1}{\sqrt{2}} \end{bmatrix} \tag{3.2}$$

The abc-to-dq transformation is defined by (3.1).

$$\begin{bmatrix} vo_d \\ vo_q \\ vo_0 \end{bmatrix} = \sqrt{\frac{2}{3}} \begin{bmatrix} cos\theta & \cos\left(\theta - \frac{2\pi}{3}\right) & \cos\left(\theta + \frac{2\pi}{3}\right) \\ -sin\theta & -\sin\left(\theta - \frac{2\pi}{3}\right) & -\sin\left(\theta + \frac{2\pi}{3}\right) \\ \frac{1}{\sqrt{2}} & \frac{1}{\sqrt{2}} & \frac{1}{\sqrt{2}} \end{bmatrix} \begin{bmatrix} vo_d \\ vo_q \\ vo_0 \end{bmatrix} \tag{3.3}$$

In this paper it is assumed that there is no path for the zero sequence components, therefore io_o in (2) and vo_0 in (4) could be ignored. However, these variables are left in the formulations to the pave the way for a more general case. The PLL form adopted here is based on aligning in closed-loop control the angle of the dq-transformation such that the voltage at the connection point has no q-axis component [7]. A PI regulator acts on the alignment error to set the rotation frequency, (5), and that frequency is integrated to give the transformation angle, (6).

$$\omega = K_P^{PLL} vo_q + K_I^{PLL} \int vo_q \, dt \tag{3.4}$$

$$\theta = \int \omega \, dt \tag{3.5}$$

To express (3.4) in a purely differential form, an additional variable is defined: $\varphi_{PLL} = \int vo_q \, dt$. This variable does not have a particular physical meaning, but it facilitates the development of the

state-space model (and has the same dimensions as magnetic flux). The additional variable is part of the state-vector together with θ (taken from (3.5)): $x_2 = [\theta \quad \varphi_{PLL}]^T$. The input variable to the PLL is $u_2 = [vo_a \quad vo_b \quad vo_c]^T$ and the output, which includes the dq transformation is $y_2 = [\theta \quad vo_d \quad vo_q]^T$. With the definitions above, the state-space model of PLL loop can then be written in the form $\dot{x}_2 = A_2 x_2 + R_2(x_2, u_2)$ as follows;

$$\dot{x}_2 = \begin{bmatrix} \dot{\theta_{PLL}} \\ \varphi_{PLL} \end{bmatrix} = A_{PLL} \begin{bmatrix} \theta_{PLL} \\ \varphi_{PLL} \end{bmatrix} + B_{PLL} \begin{bmatrix} v_{od} \\ v_{oq} \end{bmatrix} + B_{PLL2}[\Delta\omega_{com}] \tag{3.6}$$

where vo_q is given in (3.4) and is multiplication of the state variable θ with input vo_{abc}.

$$A_{PLL} = \begin{bmatrix} 0 & K_I^{PLL} \\ 0 & 0 \end{bmatrix} \quad B_{PLL} = \begin{bmatrix} 0 & K_P^{PLL} \\ 0 & 1 \end{bmatrix} \quad B_{PLL2} = \begin{bmatrix} -1 \\ 0 \end{bmatrix}$$

3.2.2 State space model of Droop Controller

Droop control allows inverters to mimic the droop characteristics of a synchronous generator. This helps a group of droop-controlled inverters to share power among themselves based on their droop coefficient and regulates the voltage and frequency of the microgrid accordingly [8]. A droop control strategy is used in the power controller to mimic the characteristics of the governor of the synchronous generator. This section presents the basics of droop control.

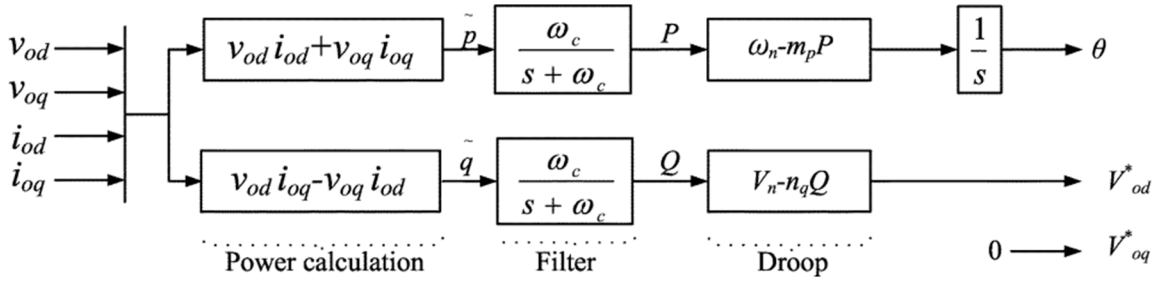

Figure 3.3. Droop Power Controller

This strategy is widely used in VSI control. The power controller sets the voltage and frequency whenever there's a load change in the system. Instantaneous real and reactive power produced by the inverter is calculated using measured output voltage and currents. This instantaneous power is then filtered using low-pass filters. In this paper it is assumed that there is no path for the zero sequence components, therefore i_{OO} in (2) and v_{OO} in (4) could be ignored. However, these variables are left in the formulation to pave the way for a more general case.

$$p = v_{od}i_{od} + v_{oq}i_{oq} \tag{3.7}$$

$$q = -v_{od}i_{od} + v_{oq}i_{oq} \tag{3.8}$$

$$P = \frac{\omega_w}{s-\omega_w}p \tag{3.9}$$

$$Q = \frac{\omega_w}{s-\omega_w}q \tag{3.10}$$

Substitute equation (3.7) & (3.8) into (3.9) & (3.10)

$$P = \frac{\omega_w}{s-\omega_w}(v_{od}i_{od} + v_{oq}i_{oq}) \tag{3.11}$$

$$Q = \frac{\omega_w}{s-\omega_w}\left(-v_{od}i_{od} + v_{oq}i_{oq}\right) \tag{3.12}$$

Then can be transformed into.

$$P(s-\omega_w) = \omega_w(v_{od}i_{od} + v_{oq}i_{oq})$$

$$Q(s-\omega_w) = \omega_w\left(-v_{od}i_{od} + v_{oq}i_{oq}\right)$$

Then expanded.

$$Ps - P\omega_w = \omega_w(v_{od}i_{od} + v_{oq}i_{oq})$$

$$Qs - Q\omega_w = \omega_w\left(-v_{od}i_{od} + v_{oq}i_{oq}\right)$$

These equations can be linearized and neglecting the higher order terms.

$$\Delta\dot{P} = -\omega_w \Delta P + \omega_w I_{od} \Delta v_{od} + \omega_w V_{od} \Delta i_{od} + \omega_w I_{oq} \Delta v_{oq} + \omega_w V_{oq} \Delta i_{oq} \tag{3.13}$$

$$\Delta\dot{Q} = -\omega_w \Delta Q - \omega_w I_{oq} \Delta v_{od} - \omega_w V_{od} \Delta i_{oq} + \omega_w I_{od} \Delta v_{oq} + \omega_w V_{oq} \Delta i_{od} \tag{3.14}$$

Real and reactive power is shared among inverters using droop equation as in (5.4), where m_P and n_Q are real and reactive power droop coefficients. The magnitude of the output voltage is given by $\sqrt{v_{od}^2 + v_{oq}^2}$ in the control strategy v_{oq} is set to zero, and thus the output voltage is aligned with d-axis.

From (1.4) & (1.5),

$$\omega = \omega_n - m_p P, \quad \dot{\theta} = \omega \tag{3.15}$$

$$v_{od} = v_n - n_q Q, \quad v_{oq} = 0 \tag{3.16}$$

$$\theta = \omega_n t + \delta$$

As discussed, earlier δ of the individual inverter is measured with respect to the common reference frame as in (3.17). The local reference frame (dq) of any one of the inverters can be chosen as the common reference frame (DQ).

$$\delta_i = \int (\omega_i - \omega_{com}) \tag{3.17}$$

$$\dot{\delta}_i = \omega_i - \omega_{com}$$

Linearizing

$$\Delta\dot{\delta}_i = \Delta\omega_i - \Delta\omega_{com} = -m_{Pi} \Delta P_i - \Delta\omega_{com} \tag{3.18}$$

Can be represented in state space form as.

$$\begin{bmatrix} \Delta\dot{\delta} \\ \Delta\dot{P} \\ \Delta\dot{Q} \end{bmatrix} = A_{PC}\begin{bmatrix} \Delta\delta \\ \Delta P \\ \Delta Q \end{bmatrix} + B_{PC1}\begin{bmatrix} \Delta i_{ldq} \\ \Delta v_{odq} \\ \Delta i_{odq} \end{bmatrix} + B_{PC2}[\omega_{com}]$$

$$\begin{bmatrix} \Delta\omega \\ \Delta v^*_{odq} \end{bmatrix} = \begin{bmatrix} C_{Pw} \\ C_{Pv} \end{bmatrix}\begin{bmatrix} \Delta\delta \\ \Delta P \\ \Delta Q \end{bmatrix} \tag{3.19}$$

Where;

$$A_{PC} = \begin{bmatrix} 0 & -m & 0 \\ 0 & -\omega_w & 0 \\ 0 & 0 & -\omega_w \end{bmatrix}$$

$$B_{PC1} = \begin{bmatrix} 0 & 0 & 0 & 0 & 0 & 0 \\ 0 & 0 & \omega_w I_{od} & \omega_w I_{oq} & \omega_w V_{od} & \omega_w V_{oq} \\ 0 & 0 & -\omega_w I_{oq} & \omega_w I_{od} & \omega_w V_{oq} & -\omega_w V_{od} \end{bmatrix}$$

$$B_{PC2} = \begin{bmatrix} -1 \\ 0 \\ 0 \end{bmatrix} \qquad C_{Pw} = [0 \quad -m_p \quad 0] \qquad C_{Pv} = \begin{bmatrix} 0 & 0 & -n_p \\ 0 & 0 & 0 \end{bmatrix}$$

3.2.3 State Space Model of Voltage & Current Controller

Reference voltage generated by the power controller is controlled using a voltage controller. The output of the voltage controller is fed to the current controller for current control. The block diagram of the voltage and current controller is shown in Fig. 3.4. Details on how to calculate the gains of voltage and the current controller can be found in [2]. The voltage controller euqations is shown in (3.20).

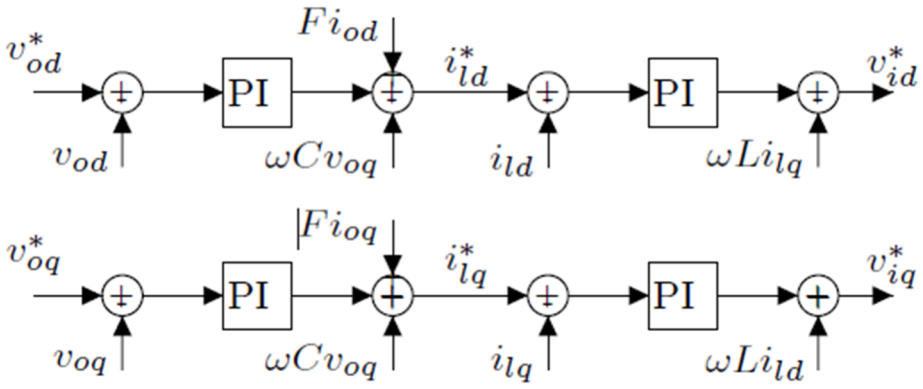

Figure 3.4. Voltage and Current controller for grid feeding inverters.

$$\dot{\emptyset}_{dq} = v_{dq\_ref}^* - v_{dq}$$

$$i_{ld}^* = Fi_{od} - w_n C_f v_{oq} + K_{pv}\left(v_{d_{ref}}^* - v_d\right) + K_{iv}\emptyset_d$$

$$i_{lq}^* = Fi_{od} + w_n C_f v_{oq} + K_{pv}\left(v_{q_{ref}}^* - v_q\right) + K_{iv}\emptyset_q \tag{3.20}$$

$$\dot{\gamma}_{dq} = i_{dq\_ref}^* - i_{dq}$$

$$v_{id}^* = K_{pc}\left(i_{d\_ref}^* - i_d\right) + K_{ic}\dot{\gamma}_d - w_n i_{lq} L_f$$

$$v_{iq}^* = K_{pc}\left(i_{q\_ref}^* - i_q\right) + K_{ic}\dot{\gamma}_q - w_n i_{ld} L_f \tag{3.21}$$

Here, the input to the subsystems is split into two terms: the reference input and the feedback inputs. Equations (3.22) – (3.23) show the states and output of voltage controller and in (3.24) – (3.25) those related to current controller are demonstrated.

$$\left[\Delta\dot{\emptyset}_{dq}\right] = A_v\left[\emptyset_{dq}\right] + B_{v1}[\Delta v_{odq}^*] + B_{v2}[\Delta x_{f,CI}] \tag{3.22}$$

$$[\Delta i^*_{ldq}] = C_v[\emptyset_{dq}] + D_{v1}[\Delta v^*_{odq}] + D_{v2}[\Delta x_{f,CI}] \quad (3.23)$$

$$[\Delta \dot{\gamma_{dq}}] = A_c[\gamma_{dq}] + B_{c1}[\Delta i^*_{ldq}] + B_{c2}[\Delta x_{f,CI}] \quad (3.24)$$

$$[\Delta v^*_{ldq}] = C_c[\gamma_{dq}] + D_{c1}[\Delta i^*_{ldq}] + D_{c2}[\Delta x_{f,CI}] \quad (3.25)$$

φ_{dq} and γ_{dq} are auxiliary state variables, which measure the variation of voltage and current (vo_{dg} ,il_{dq}) from the reference values. vi and ii are the voltage and current of DC/AC inverter, V_o is the voltage measured after LC filter and io is the current of coupling inductance. These variables are depicted in Figure 3.3. k_{pv} and k_{iv} are the parameters of PI inside the voltage controller and kpc and k_{ic} are those related to the current controller PI. R_f, C_f and L_f are also parameters of LC filter.

$$\Delta\emptyset_{dq} = \begin{bmatrix}\Delta\emptyset_d \\ \Delta\emptyset_q\end{bmatrix}$$

$$B_{v1} = \begin{bmatrix}1 & 0 \\ 0 & 1\end{bmatrix}, B_{v1} = \begin{bmatrix}0 & 0 & -1 & 0 & 0 & 0 \\ 0 & 0 & 0 & -1 & 0 & 0\end{bmatrix}$$

$$C_v = \begin{bmatrix}K_{iv} & 0 \\ 0 & K_{iv}\end{bmatrix}, \; D_{v1} = \begin{bmatrix}K_{pv} & 0 \\ 0 & K_{pv}\end{bmatrix}$$

$$D_{v2} = \begin{bmatrix}0 & 0 & -K_{pv} & -w_n C_f & 0 & 0 \\ 0 & 0 & w_n C_f & -K_{pv} & 0 & 0\end{bmatrix}$$

$$\Delta\gamma_{dq} = \begin{bmatrix} \Delta\gamma_d \\ \Delta\gamma_q \end{bmatrix}$$

$$B_{c1} = \begin{bmatrix} 1 & 0 \\ 0 & 1 \end{bmatrix}, B_{c2} = \begin{bmatrix} -1 & 0 & 0 & 0 & 0 & 0 \\ 0 & -1 & 0 & 0 & 0 & 0 \end{bmatrix}$$

$$C_v = \begin{bmatrix} K_{ic} & 0 \\ 0 & K_{ic} \end{bmatrix}, \; D_{v1} = \begin{bmatrix} K_{pc} & 0 \\ 0 & K_{pc} \end{bmatrix}$$

$$D_{v2} = \begin{bmatrix} -K_{pc} & -w_n L_f & 0 & 0 & 0 & 0 \\ w_n L_f & -K_{pc} & 0 & 0 & 0 & 0 \end{bmatrix}$$

3.2.4 State Space Model of Time Delay

Time delay arises in a wide range of practical engineering applications such as signal processing, fibre optics research, and VSI circuit design. The subject of delay and its analysis has already received much attention in these areas. [6] Time delay modeling was described in the earlier chapter. Low Pass filter was used to emulate the time delay that's common in the GFM controller devices. Figure 3.4 depicts a simple network control system that's incurs with several delay. Time delays caused by transmission and process of the remote signals within the wide-area measurement system can vary from tens to several hundreds of milliseconds. If the time delay effects are taken into consideration, a power system equipped with wide area damping controllers would results in stability affecting the robustness of the GFM.

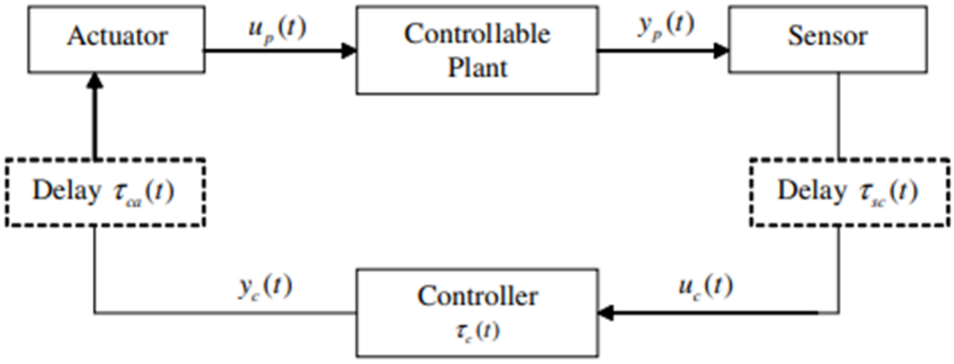

Figure 3.5 Network Control System

By combining the delay, we generate a model expression for the time delay.

$$V_i^s = e^{-sT_d} V_T^s$$

$$V_i^s = \left(\frac{1}{T_d s+1}\right) V_T^s \tag{3.26}$$

This equation is then being express in the time domain as;

$$\frac{dx_{dq}^s}{dt} = A_T \begin{bmatrix} x_d \\ x_q \end{bmatrix} + B_T \begin{bmatrix} V_{Td} \\ V_{Tq} \end{bmatrix} \tag{3.27}$$

$$V_T = C_T \begin{bmatrix} x_d \\ x_q \end{bmatrix} + D_T \begin{bmatrix} V_{Td} \\ V_{Tq} \end{bmatrix}$$

Where x_d & x_q is the state variable and V_{Tdq} is the input vectors.

$$A_T = \begin{bmatrix} -\frac{1}{T_d} & 0 \\ 0 & -\frac{1}{T_d} \end{bmatrix} \quad B_T = \begin{bmatrix} 1 & 0 \\ 0 & 1 \end{bmatrix} \quad C_T = \begin{bmatrix} \frac{1}{T_d} & 0 \\ 0 & \frac{1}{T_d} \end{bmatrix} \quad D_T = \begin{bmatrix} 0 & 0 \\ 0 & 0 \end{bmatrix}$$

After modelling the agreement time delay based on the communication's speed of the network, it is important to consider the controller time delay. The whole microgrid has a threshold for delay.

So, it should be noted that the total time delay of agreement and controller should not exceed this threshold.

3.2.5 State Space model of LCL filter

The state space model for the output filter and the coupling inductance, shown in 3.34, can be formed by use of equations 3.28 – 3.33 considering that the GFM can provide the reference voltage.

Output equation for LCL filter in dq-frame are represented as:

$$\frac{di_{ld}}{d_t} = \frac{-r_f}{L_f} i_{ld} + \omega i_{lq} + \frac{1}{L_f} v_{id} - \frac{1}{L_f} v_{od} \tag{3.28}$$

$$\frac{di_{lq}}{d_t} = -\frac{r_f}{L_f} i_{lq} - \omega i_{ld} + \frac{1}{L_f} v_{iq} - \frac{1}{L_f} v_{oq} \tag{3.29}$$

$$\frac{dv_{od}}{d_t} = \omega v_{oq} + \frac{1}{C_f} i_{ld} - \frac{t_r}{2C_f} i_{od} \tag{3.30}$$

$$\frac{dv_{oq}}{d_t} = -\omega v_{od} + \frac{1}{C_f} i_{lq} - \frac{1}{C_f} i_{oq} \tag{3.31}$$

$$\frac{di_{od}}{d_t} = -\frac{r_c}{L_c} i_{od} + \omega i_{oq} + \frac{1}{L_c} v_{od} - \frac{1}{L_c} v_{bd} \tag{3.32}$$

$$\frac{di_{oq}}{d_t} = -\frac{r_c}{L_c} i_{oq} + \omega i_{od} + \frac{1}{L_c} v_{oq} - \frac{1}{L_c} v_{bq} \tag{3.33}$$

These equation above are the first step in modeling the LCL filter system. This can be linearized around the operating point and re-written in state space form as below;

$$\begin{bmatrix} \Delta \dot{i}_{ldq} \\ \Delta \dot{v}_{odq} \\ \Delta \dot{i}_{odq} \end{bmatrix} = [A_{LCL}] \begin{bmatrix} \Delta i_{ldq} \\ \Delta v_{odq} \\ \Delta i_{odq} \end{bmatrix} + [B_{LCL}][\Delta v_{idq}] + [B_{LCL2}][\Delta v_{bdq}] + [B_{LCL3}][\Delta \omega] \tag{3.34}$$

Where,

$$A_{LCL} = \begin{bmatrix} -\frac{r_f}{L_f} & \omega & \frac{1}{L_f} & 0 & 0 & 0 \\ -\omega & -\frac{r_f}{L_f} & 0 & \frac{1}{L_f} & 0 & 0 \\ \frac{1}{C_f} & 0 & 0 & \omega & -\frac{1}{C_f} & 0 \\ \frac{1}{C_f} & 0 & -\omega & 0 & 0 & -\frac{1}{C_f} \\ 0 & 0 & \frac{1}{L_c} & 0 & -\frac{r_c}{L_c} & \omega \\ 0 & 0 & 0 & \frac{1}{L_c} & -\omega & -\frac{r_c}{L_c} \end{bmatrix}$$

$$B_{LCL} = \begin{bmatrix} \frac{1}{L_f} & 0 \\ 0 & \frac{1}{L_f} \\ 0 & 0 \\ 0 & 0 \\ 0 & 0 \\ 0 & 0 \end{bmatrix} \qquad B_{LCL2} = \begin{bmatrix} 0 & 0 \\ 0 & 0 \\ 0 & 0 \\ 0 & 0 \\ -\frac{1}{L_c} & 0 \\ 0 & -\frac{1}{L_c} \end{bmatrix}$$

$$B_{LCL3} = [I_{lq} - I_{ld}\ V_{oq} - V_{od}\ I_{oq} - I_{od}]^T$$

3.3 Model of Inverter

As explained previously, once we have defined our state variables for our controller and concatenate them. To connect the VSI inverters to a microgrid, all output currents and voltages need to be expressed in a common reference frame. So, here the Δi_{odq} will be converted to the Δi_{oDQ} by use of the transformation technique given in equation 3.1.

$$\left[\Delta i_{oDQ}\right] = [T_s]\left[\Delta i_{odq}\right] + [T_C][\Delta\delta] \tag{3.35}$$

Where

$$T_s = \begin{bmatrix} \cos(\delta_0) & -\sin(\delta_0) \\ \sin(\delta_0) & \cos(\delta_0) \end{bmatrix}$$

$$T_c = \begin{bmatrix} -I_{od}\sin(\delta_0) & -I_{oq}\cos(\delta_0) \\ I_{od}\cos(\delta_0) & -I_{oq}\sin(\delta_0) \end{bmatrix}$$

Similarly, the input signal to the inverter model is the bus voltage which is expressed on the common reference frame. The bus voltage can be converted to the individual inverter reference frame using reverse transformation, given by;

$$[\Delta v_{bdq}] = [T_s^{-1}][\Delta v_{bDQ}] + [T_V^{-1}][\Delta\delta] \tag{3.36}$$

Where

$$[T_V^{-1}] = \begin{bmatrix} -V_{bD}\sin(\delta_0) & V_{bQ}\cos(\delta_0) \\ -V_{bD}\cos(\delta_0) & -V_{bQ}\sin(\delta_0) \end{bmatrix}$$

Finally, after merging all previous state equations, the model of one VSI inverter will be organized as in 3.64. After building the state space model for each VSI inverter, they can be added up to form a unit model for all the VSI inverters. A complete state-space small-signal model of the inverter can be obtained by combining the state-space models of the, phase lock loop, power controller, voltage controller, current controller and output LCL filter, given by (3.6), (3.19), (3.22), (3.23), (3.24), (3.25), (3.27), and (3.34). There are totally 17 states, two inputs, and two outputs in each individual inverter model (except the inverter whose reference frame is the common reference frame, which has three outputs).

$$[\Delta\dot{x}_{inv}] = A_{inv}[\Delta x_{inv}] + B_{inv}[\Delta v_{bDQ}] + B_{iwcom}[\Delta\omega_{com}] \tag{3.37}$$

$$\begin{bmatrix} \Delta\omega \\ \Delta i_{oDQ} \end{bmatrix} = \begin{bmatrix} C_{INV\omega} \\ C_{INVc} \end{bmatrix} [\Delta x_{inv}]$$

Where,

$$\Delta x_{inv} = [\Delta\theta\ \Delta\varphi_{PLL}\ \ \Delta\delta\ \Delta P\ \Delta Q\ \Delta\emptyset_{dq}\ \Delta\gamma_{dq}\ \Delta x_{dq}\ \ \Delta i_{ldq}\ \Delta v_{odq}\ \Delta i_{odq}]^T$$

$$\Delta v_{bDQ} = [\ \Delta v_{bD}\ \Delta v_{bQ}]^T$$

$$A_{inv} = \begin{bmatrix} A_{PLL} & 0 & 0 & 0 & 0 & B_{PLL} \\ 0 & A_P & 0 & 0 & 0 & B_P \\ 0 & B_{v1}C_{pv} & 0 & 0 & 0 & B_{v2} \\ 0 & B_{c1}D_{v1}C_{pv} & B_{c1}C_v & 0 & 0 & B_{c1}D_{v2} + B_{c2} \\ 0 & B_tD_{c1}D_{v1}C_{pv} & B_tD_{c1}C_v & B_tC_c & A_t & B_tD_{c2} + B_tD_{c1}D_{v2} \\ 0 & B_{lcl1}D_tD_{c1}D_{v1}C_{pv} + B_{lcl2}T_{vinv} + B_{lcl3}C_{pw} & B_{lcl1}D_tD_{c1}C_v & B_{lcl1}D_tC_c & B_{lcl1}C_t & A_{lcl} + B_{lcl1}(D_tD_{c1}D_{v2} + D_tD_{c2}) \end{bmatrix}$$

$$B_{inv} = [\ 0\ 0\ 0\ 0\ 0\ \ B_{lcl2}T_s^{-1}]^T$$

$$B_{iwcom} = [\ B_{Pwcom}\ 0\ 0\ 0\ 0\ 0]^T$$

$$C_{invw} = [\ C_{Pwcom}\ 0\ 0\ 0\ 0\ 0]$$

$$C_{invc} = [\ [T_c 0\ 0]\ 0\ 0\ [0\ 0\ T_s]$$

3.3.1 Model of Line

Small-signal state-space equation of lines on a common reference frame is represented by (3.38). A detailed modeling of network is given in [8].

$$[\Delta\dot{x_{NET}}] = [A_{NET}][\Delta x_{NET}] + [B_{1_{NET}}][\Delta v_{bDQ}] + [B_{2_{NET}}][\Delta\omega] \quad (3.38)$$

3.3.2 Load Modeling

A typical RL load is used in this study. Small-signal state-space equation of loads on a common reference frame can be represented by (3.39). A detailed load modeling is given in [8].

$$[\Delta\dot{x_{LOAD}}] = [A_{LOAD}][\Delta x_{LOAD}] + [B_{1_{LOAD}}][\Delta v_{bDQ}] + [B_{2_{LOAD}}][\Delta\omega] \quad (3.39)$$

3.4 Microgrid Model

A complete model of a microgrid comprising inverters, lines, and loads is presented in this section. Irrespective of the control type, an inverter has a power section and a control section. The power section comprises of the inverter, output filter, and coupling inductor. At the same time, the control

section includes a power controller, voltage controller (absent for grid feeding inverters), and current controller. Modeling of the power and controller for each type of inverter is presented. The dynamics of RL line are modelled. A general RL type of load is considered for load modeling.

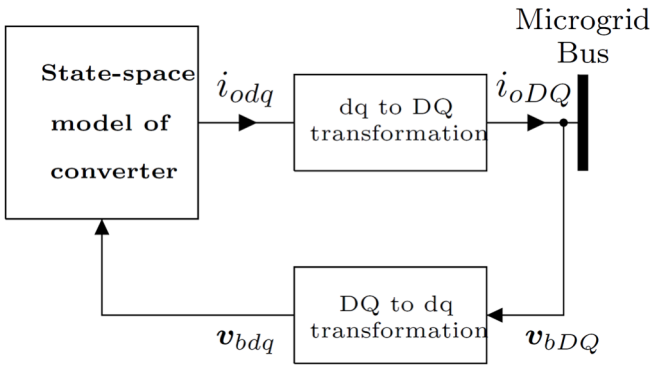

Figure 3.6 Variable transformation for grid forming inverter.

As seen from figure 3.6 the state-space model of GFM inverter, network, and load, each of them has bus voltage as input. Value of i_{th} bus voltage $\Delta Vb_{DQ}i$ should be well defined by choosing high value of r_N, such that its effect on dynamic stability of system is minimum.

$$v_{bDi} = r_N(i_{oDi} - i_{LoadDi} + i_{lineDi})$$

$$v_{bQi} = r_N(i_{oQi} - i_{LoadQi} + i_{lineQi}) \tag{3.40}$$

For a microgrid system Δv_{bDQ} is given by.

$$[\Delta v_{bDQ}] = R_N(M_{inv}[\Delta i_{oDQ}] + M_{load}[\Delta i_{loadDQ}] + M_{net}[\Delta i_{lineDQ}]) \tag{3.41}$$

Matrices M_{INV}, M_{LOAD} and M_{NET} are mapping matrices defined in [3]. Combining (3.37), (3.38),(3.39) and (3.41) a complete microgrid system matrix can be obtained as:

$$[\Delta x_{mg}] = [A_{mg}][\Delta x_{mg}] \tag{3.42}$$

Where,

$$[\Delta x_{mg}] = [\Delta x_{INV}\ \Delta x_{NET}\ \Delta x_{LOAD}]$$

$$[A_{mg}] = \begin{bmatrix} A_{INV} + B_{INV}R_N M_{INV} C_{INVc} & B_{INV}R_N M_{NET} & B_{INV}R_N M_{LOAD} \\ B_{1NET}R_N M_{INV} C_{INVc} + B_{2NET} C_{INVw} & A_{NET} + B_{1NET}R_N M_{NET} & B_{1NET}R_N M_{LOAD} \\ B_{1LOAD}R_N M_{INV} C_{INVc} + B_{2LOAD} C_{INVw} & B_{1LOAD}R_N M_{NET} & A_{LOAD} + B_{1LOAD}R_N M_{LOAD} \end{bmatrix}$$

3.5 Conclusions

A unified state-space model microgrid system was established, which was used to analyse the system stability in terms of parameter variation. Small-signal stability limits were established based on the model, which was verified by simulation results. Such established limits are useful in the current deregulated market where each customer can have their own type of inverter control. And hence having an analysis based on inverter parameters helps to ensure system stability. The established stability criterion was extended to IEEE-9 bus system, which will be discussed in chapter 4.

CHAPTER 4

SMALL-SIGNAL STABILITY ANALYSIS OF VSIs IN A MICROGRID

4.1 Introduction

Due to the climate change crisis, there is a growing concern to make electrical energy a carbon-free source of energy. This leads to an increase in the penetration of renewable sources of energy such as solar and wind in the power system. The ability to install these renewable sources closer to the load has led to the emergence of a more flexible and reliable small-scale power system called a microgrid. As discussed previously, these renewable sources are interfaced with the microgrid by power electronic devices. This implies that the microgrid lacks inertia and thus its control involves a fast control of voltage and frequency. In addition, a fast control requires fast measurements that are noisy, and thus a microgrid control poses a significant stability concern for a microgrid system operator. A microgrid is subjected to both small-signal and large-signal disturbances. Nonetheless, microgrid stability studies are focused on small-signal disturbances. So far, this thesis has also covered small-signal modeling and analysis of a microgrid. A major drawback of using a small-signal stability approach is that the results are only valid for the small neighbourhood of the operating point. Hence, the use of the small-signal model for large deviations from the operating point will yield the wrong analysis.

4.2 Eigenvalue and Sensitivity Analysis of Microgrid Inverter

From chapter 2, the derived state space model small signal analysis was tested. The objective of the study is to find the eigenvalues which are critical to system stability and find a correlation between the droop inverter gains to establish operating conditions for system stability. Base parameters and test conditions was used in [19].

The eigenvalue concept of control theory has been extensively used to determine the stability of conventional power systems. Eigenvalues, termed modes, are the solution of the characteristic equation of a system's linearized state matrix. Eigenvalues reveal the different frequency components in the system and their available damping.

Table I Test System Parameters

Inverter Parameters (10kVA rating)		
Parameters	Value	Units
f_s	8	kHz
L_f	1.35	mH
C_f	50	uF
r_f	0.1	Ω
L_c	0.35	mH
r_{Lc}	0.03	Ω
ω_c	31.41	rad/s
m_p	9.4e-5	-
n_q	1.3e-3	-
K_{pv}	0.05	-
K_{iv}	390	-
K_{pc}	10.5	-
K_{ic}	16e3	-
F	0.75	-
r_{line1}	0.23	Ω
r_{line2}	0.35	Ω
x_{line1}	0.1	Ω
x_{line2}	0.58	Ω

Table II Initial Conditions

Parameters	Value	Units
V_{od}	[380.8 381.8 380.4]	V
V_{oq}	[0 0 0]	V
I_{od}	[11.4 11.4 11.4]	A
I_{oq}	[0.4 -1.45 1.25]	A
I_{ld}	[11.4 11.4 11.4]	rad/s
I_{lq}	[-5.5 -7.3 -4.6]	A
V_{bd}	[379.5 380.5 379]	V
V_{bq}	[-6 -6 -5]	V
ω_0	[376.99]	rad/s
δ_0	[0 1.9e-3 -0.0113]	-
I_{line1d}	[-3.8]	A
I_{line1q}	[0.4]	A
I_{line2d}	[7.6]	A
I_{line2q}	[-1.3]	A

The proportional and integral gains of the voltage controller, shown in Table I, were chosen using classical pole-zero and bode techniques to yield a bandwidth of 400 Hz for the voltage controller. The current feed-forward gain was chosen to yield a low output impedance and hence improve the disturbance rejection of the inverter system. The current controller was designed for 1.6-kHz bandwidth with good rejection of high-frequency disturbance. Although, the control was

implemented in the discrete-time domain, the equivalent continuous domain gains are provided (in Table I) for construction of the model.

A complete model of the test system was obtained using the procedure outlined in chapter 3. Initial conditions of the system are given in Table II. However, it is possible to use a more general load-flow solution as is often done in conventional power system modeling to obtain initial steady-state conditions. The value chosen for virtual resistor $r_N$was 1000Ω.

The objective of the study is to find the eigenvalues which are critical to system stability and find a correlation between the droop inverter, VSG, and PQ inverter gains to establish operating conditions for system stability. Table III shows the eigenvalues for the grid forming inverter without considering time delay and PLL model. These values are now compared to Table VI with the grid forming inverter considering the time delay and PLL model. These

Table III. Eigen Vectors with Participation Factors w/o Time Delay & PLL

Mode	Eigen Values (1e3)	Participation Factor
1	-2.9021 + 8.5143i	$\Delta v_{oq}, \Delta i_{od}$
2	-2.9021 - 8.5143i	$\Delta v_{od}, \Delta i_{iq}$
3	-2.7842 + 7.9623i	$\Delta v_{od}, \Delta i_{lq}$
4	-2.7842 - 7.9623i	$\Delta v_{od}, \Delta i_{lq}$
5	-1.1228 + 1.5084i	$\Delta v_{oq}, \Delta i_{od}$
6	-1.1228 - 1.5084i	$\Delta \emptyset_q, \Delta \gamma_d$
7	-1.0974 + 1.4740i	$\Delta v_{oq}, \Delta i_{od}$
8	-1.0974 - 1.4740i	$\Delta v_{oq}, \Delta i_{od}$
9	-0.0529 + 0.0957i	$\Delta i_{lq}, \Delta \gamma_q$
10	-0.0529 - 0.0957i	$\Delta \delta, \Delta P$
11	-0.0010 + 0.0633i	$\Delta v_{od}, \Delta i_{lq}$
12	-0.0010 - 0.0633i	$\Delta i_{lq}, \Delta \gamma_q$
13	-0.0173 + 0.0000i	$\Delta \delta, \Delta P$

Table VI. Eigen Vectors with Participation Factors with Time Delay & PLL

Mode	Eigen Values (1e4)	Participation Factor
1	-9.2181 + 0.0313i	$\Delta v_{od}, \Delta i_{oq}$
2	-9.2181 - 0.0313i	$\Delta v_{od}, \Delta i_{oq}$
3	-0.3348 + 2.5262i	$\Delta v_{od}, \Delta i_{oq}$
4	-0.3348 - 2.5262i	$\Delta v_{od}, \Delta i_{oq}$
5	-0.3319 + 2.4637i	$\Delta v_{od}, \Delta \emptyset_q$
6	-0.3319 - 2.4637i	$\Delta v_{od}, \Delta \emptyset_q$
7	-0.1020 + 0.1432i	$\Delta v_{oq}, \Delta x_q$
8	-0.1020 - 0.1432i	$\Delta Q, \Delta \emptyset_d$
9	-0.1018 + 0.1419i	$\Delta Q, \Delta \emptyset_d$
10	-0.1018 - 0.1419i	$\Delta \delta, \Delta i_{oq}$
11	-0.0088 + 0.0047i	$\Delta \gamma_q, \Delta \gamma_d$
12	-0.0088 - 0.0047i	$\Delta P, \Delta Q$
13	-0.0004 + 0.0058i	$\Delta v_{od}, \Delta v_{oq}$
14	-0.0004 - 0.0058i	$\Delta v_{od}, \Delta v_{oq}$
15	-0.0003 + 0.0000i	$\Delta P, \Delta Q$

Figure 4.1 shows the complete eigenvalues of the system for the initial conditions given in Table II. It can be seen that a large range of frequency components exist and that these fall in to three different clusters. This shows us that the different stages of the eigen values obtain and their respective participations. When comparing these values to Figure 4.2. This analysis shows that the high frequency modes in cluster “3” are sensitive to the state variables of LCL filter block of inverters and the line currents. The modes in cluster “2” are largely sensitive to the state variables of voltage controller, current controller, and output filter. The low frequency dominant modes shown in cluster “1” are largely sensitive to the state variables of the power controller. However, these modes are also sensitive to the reactive power. This a consequence of the coupling of real and reactive powers in the network due to presence of highly resistive lines.

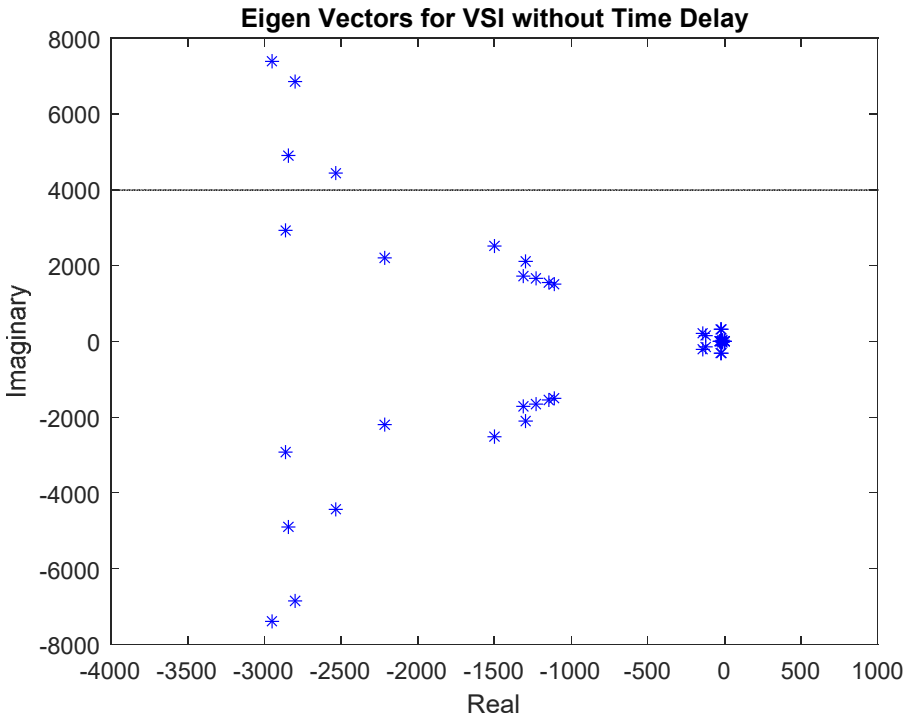

Figure 4.1 Eigen vectors for VSI without Time Delay & PLL

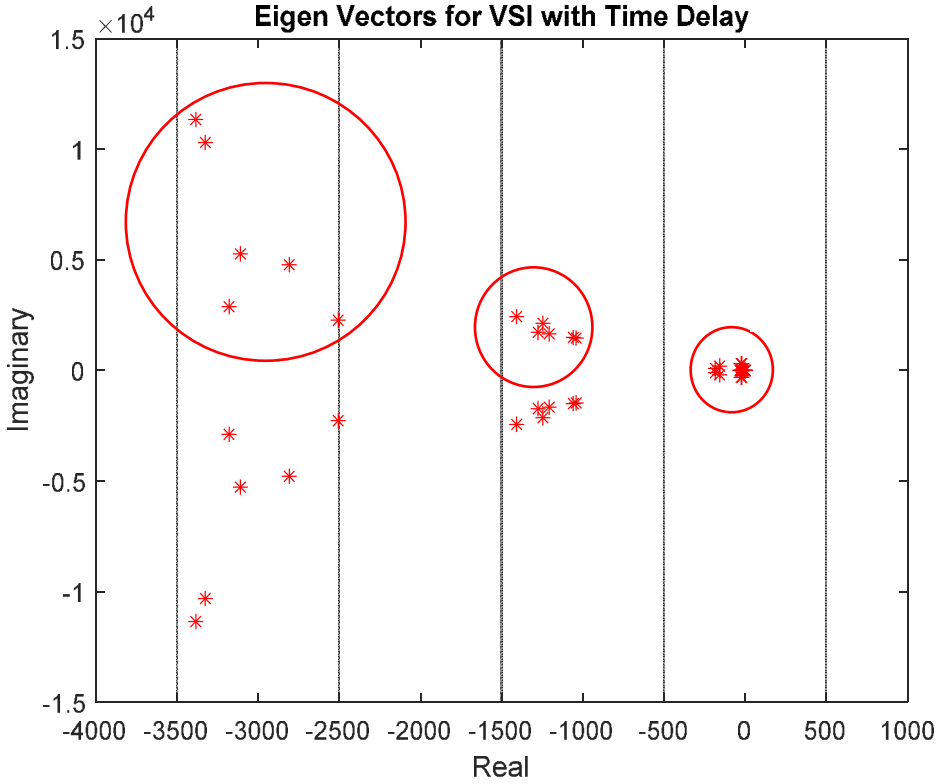

Figure 4.2 Eigenvalue spectrum of the system indicates various modes.

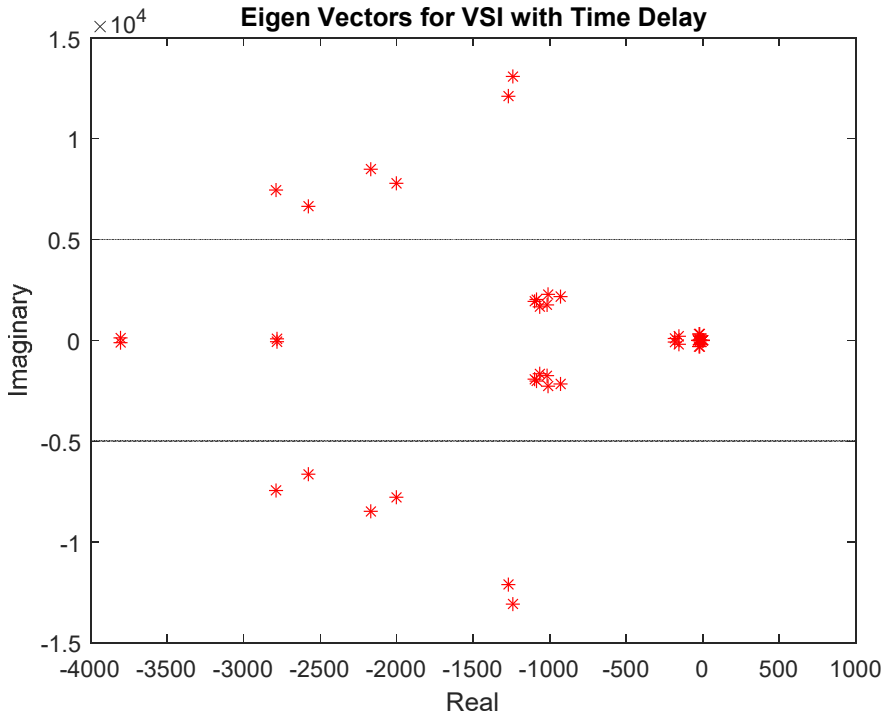

Figure 4.3 Eigen vectors for VSI with Time Delay & PLL @Time Delay 0.1ms

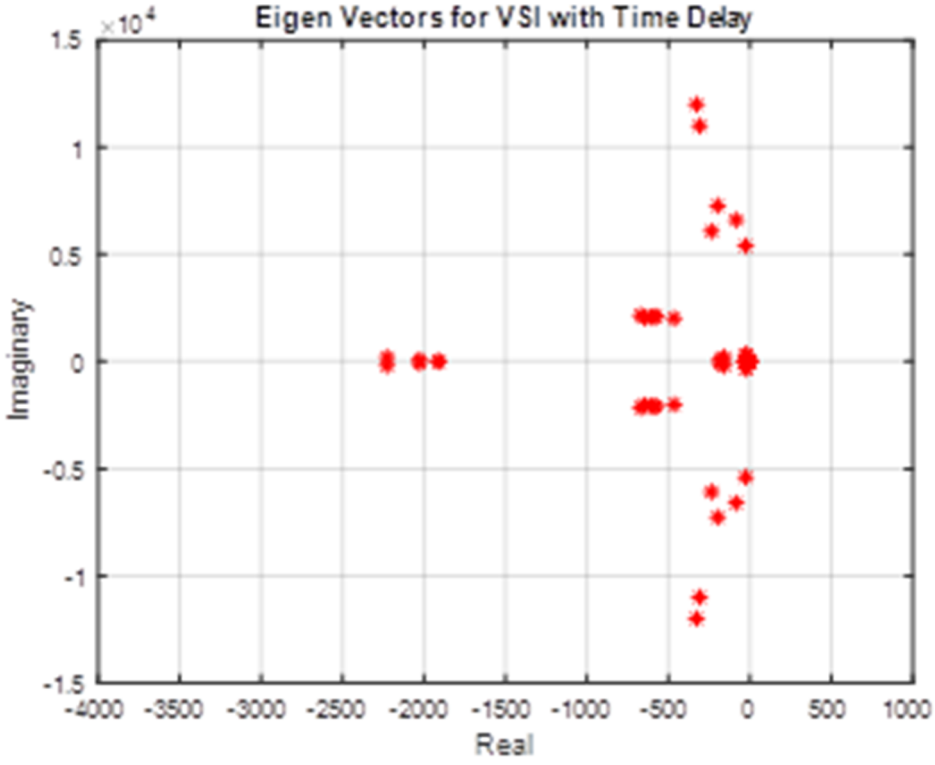

Figure 4.4 Eigen vectors for VSI with Time Delay & PLL @Time Delay 0.5ms

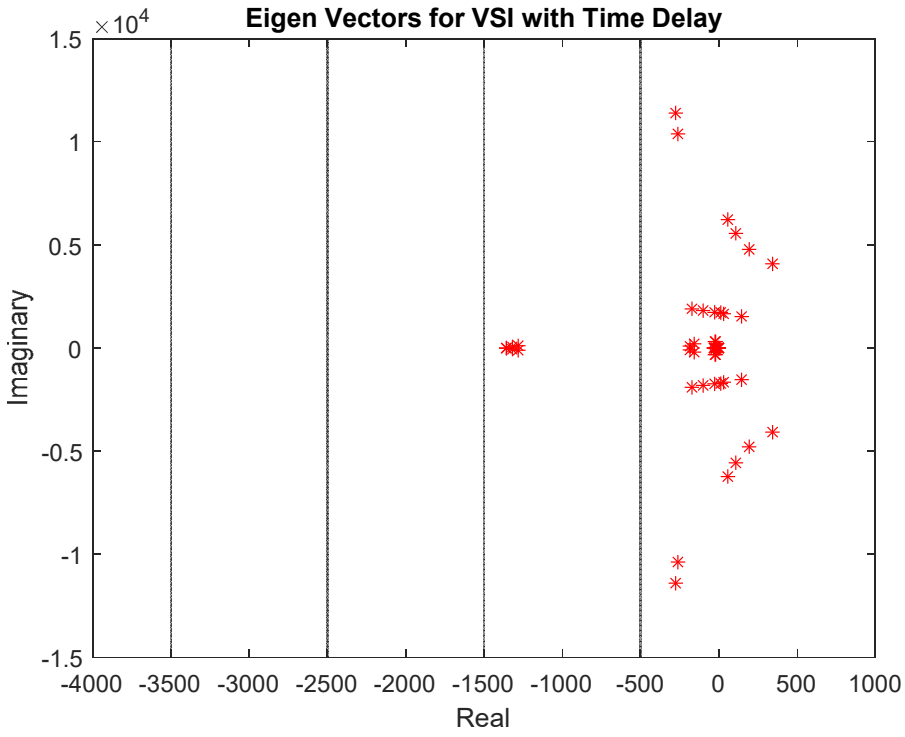

Figure 4.5 Eigen vectors for VSI with Time Delay & PLL @Time Delay 1ms

4.3 Testing Conditions and requirement of Distribution Energy Resources (DER)

MATLAB/Simulink contains a micro inverter model that are comprised of three parallel inverter components. The eigenvalues of the state space model are depicted in Figure 4.2-4.4 with the inverter's time delay involvement in supplying the demand. The communication link is assumed to be perfect without any loss or delay as shown in Figure 4.1.

In the Simulink, we test a case with the parallel Operations bus system, to verify the impact of time delay in our model. Our anticipation is that, as the time delay increase, we will notice a variation in frequency and voltage on the grid. A test will be conducted with this system under three conditions.

1. No Load changes.
2. Increase Load

3. Disturbance
    a. Line- Ground Fault
    b. Line to Line Fault

Firstly, we must define a few parameters within out test. For this we use the IEEE – 1547. 2018 standard. This standard has been adopted by a few states, such as California and Texas. Now, there are more states that are considering this adoption soon. This standard establishes criteria and requirements for interconnection of distributed energy resources with electric power systems (EPSs) and associated interfaces. The stated technical specifications and requirements are universally needed for interconnection and interoperability of distributed energy resources (DERs) and will be sufficient for most installations. The specified performance requirements apply at the time of interconnection and if the DER remains in service. A DER must trip for any short-circuit faults on the circuit to which it is connected.

- Exception for faults not detectable by Area EPS protection.
- At Area EPS Operator discretion, sequential tripping can be employed.

DER must detect and cease to energize for open phase condition directly at the reference point of applicability within two seconds.

DER must implement means such that Area EPS circuit reclosing does not result in unacceptable stress or disturbance. Possible means include:

- Low DER penetration = no islanding sustained for reclose delay
- Feeder reclosing “hot-line blocking”
- Transfer trip
- Anti-islanding detection proven to be faster than reclose delay.

In this case, we are concerned with the frequency conditions DERs must ride through. If the frequency remains in the continuous operations or ride-through frequency range, DER shall not trip for the rate of change of frequency (ROCOF) criterion;

Table V. IEEE 1547-2018 Frequency Requirement

Conditions:	Frequency Level:	Durations
Over-Frequency	61.8-66.0 Hz	0.16s-1.0s
Under-Frequency	50.0-57.0 Hz	
Over-Frequency	61.8-66.0 Hz	180s-1000s
Under-Frequency	50.0-59.0 Hz	

For this test we are focus on Category III. Which requires DER voltage/frequency ride-through for all bulk system needs with considerations of fault-induced delayed voltage recovery (FIDVR). Category II mandatorily requires momentary cessation. This is described in Figure 4.3 & 4.4

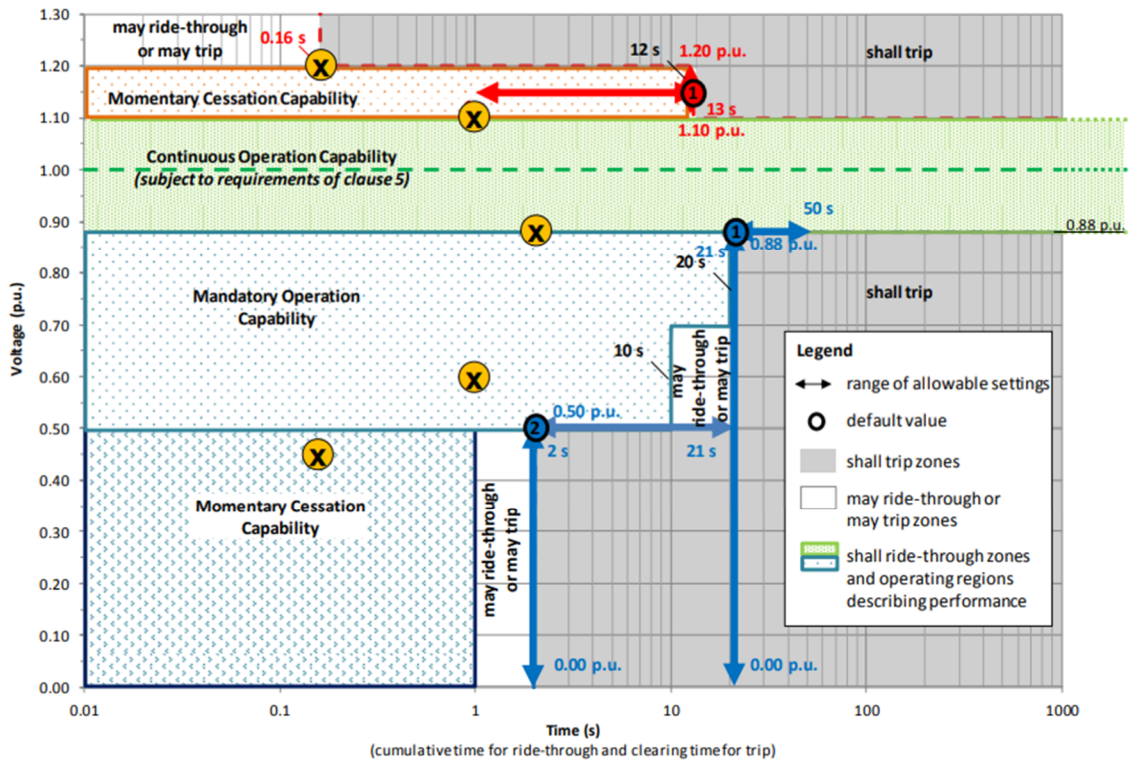

Figure 4.5. Actual Abnormal Voltage Requirements for Category III.

Figure 4.3 describes the over and under voltage trip levels. And this is the testing using the conditions within the Momentary Cessation Capability, would provide a better representation of the results we are looking for in our model. By understanding the nominal conditions set for these IBR would provide adequate results and expected conclusions.

For example.

- If feeder is faulted and tripped at the substation, then DER in momentary cessation will not energize the islanded feeder.
- DER will eventually trip off if grid voltage does not return.

We expected a suitable range for our time delay to be between 0.01 seconds to 1 second. This will be used in our Simulink model.

Similarly, the frequency ride through capabilities plays an important role as described in chapter 2. Figure 4.4 provides a detail outline for the conditions. This figure describes the two over and underfrequency trip levels. The range of allowable settings defines such that some IEEE Std 1547a-2014 default settings cannot be accommodated.

This function is per IEEE Std 1547-2018 not to be disabled, adjust dead bands and droop if necessary – Only a functional capability requirement – Utilization remains outside the scope of IEEE 1547-2018 – Over frequency: all DERs required to provide droop response – Underfrequency: No requirement to maintain operational headroom. Moreover, from this standard of measurements. This criterion will be used to test the validity of our eigen values found in chapter 4.

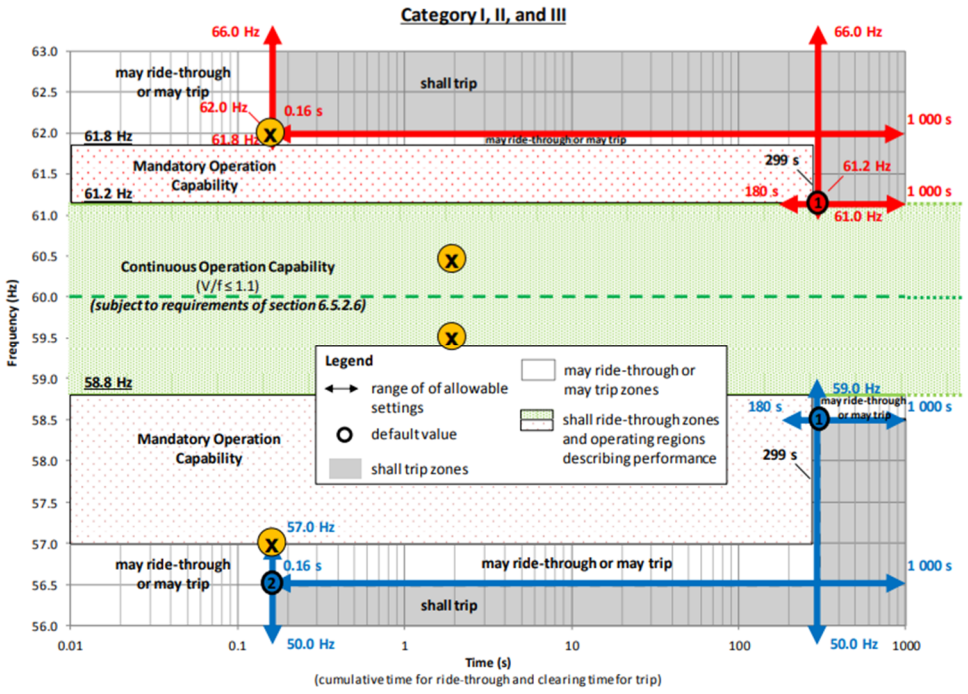

Figure 4.6 Actual Abnormal Frequency Requirements.

4.4 Implementing the System function in MATLAB/Simulink

The state-space model in (3.23) is developed in MATLAB by considering the PCC voltage as the only input. Based on the estimated VSI currents the duty cycle inputs for the same sate space model are computed using the open-loop model (1). The state-space model results are compared with 30 kW VSI circuit model developed in MATLAB/Simulink running at a sample time of 50µs and switching frequency of 27kHz is used for VSI operation. The control application that includes current, voltage and droop controllers are running at 50 µs sample time. The model will consist of three parallel inverters as designed in chapter 3. These inverters are controlled by a micro supervisory system which contains the phase lock loop system. The time delay function was emulated by the transport function in the Simulink library. The Droop controller, voltage controller, & current controller was designed to the specifications as shown in chapter 3. The model is as shown in figure 4.5. The three parallel inverters have a power rating of 10kW. Each inverter is identical, meaning that they all have same droop control settings and gains. These inverters are connected to the point of common coupling (PCC) with three different load condition

and a fault condition. (1) Load one is a resistive & inductive load. (2) Load 2 is a purely resistive load. (3) Load 3 is a varying load. (4) A fault disturbance will be placed on the load. While varying the time delay in four parts; 0 delay, 0.01s delay, 0.1s delay & 1s delay. In each case, the frequency, voltage and output power will record. To validate our findings in the early section of chapter 4, is it expected that as the delay is increase, we will begin to see instability in the voltage and frequency. The instability of these two components, has been discussed in chapter 2.

To check for instability, table I in this chapter will be used. Along with figure 4.3 & 4.4. The inverter switching frequency is set to 27kHz, which is a suitable range for a MOSFET device. The DC link voltage is set to 1kV. The secondary line voltage after the LCL system is 480V. Since no switching devices can operate effectively in a distribution system at MV/ HV voltage levels. A transformer is placed in the model. This is seen in Figure 4.6.

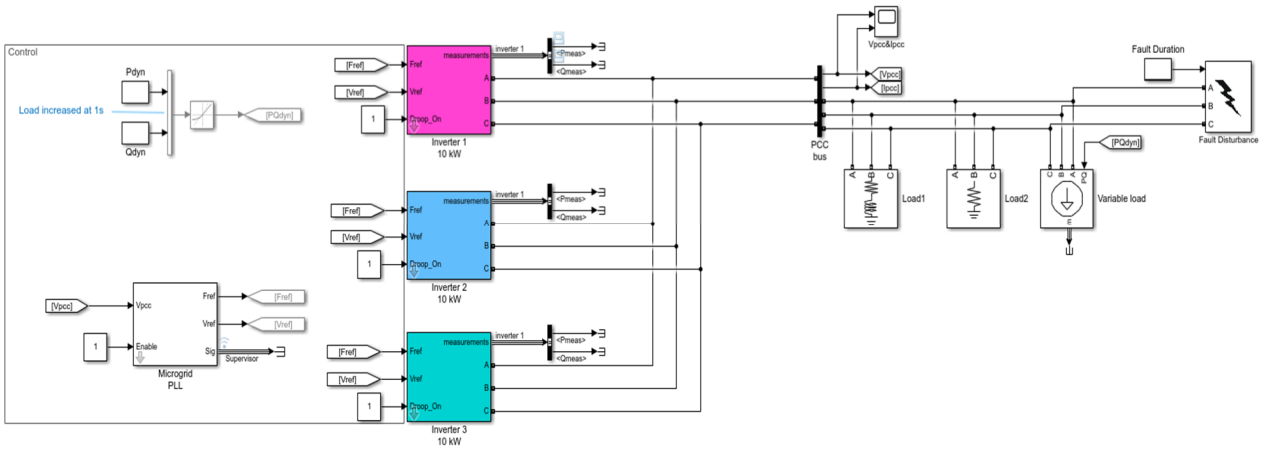

Figure 4.7 30kW Parallel GFM Inverters System

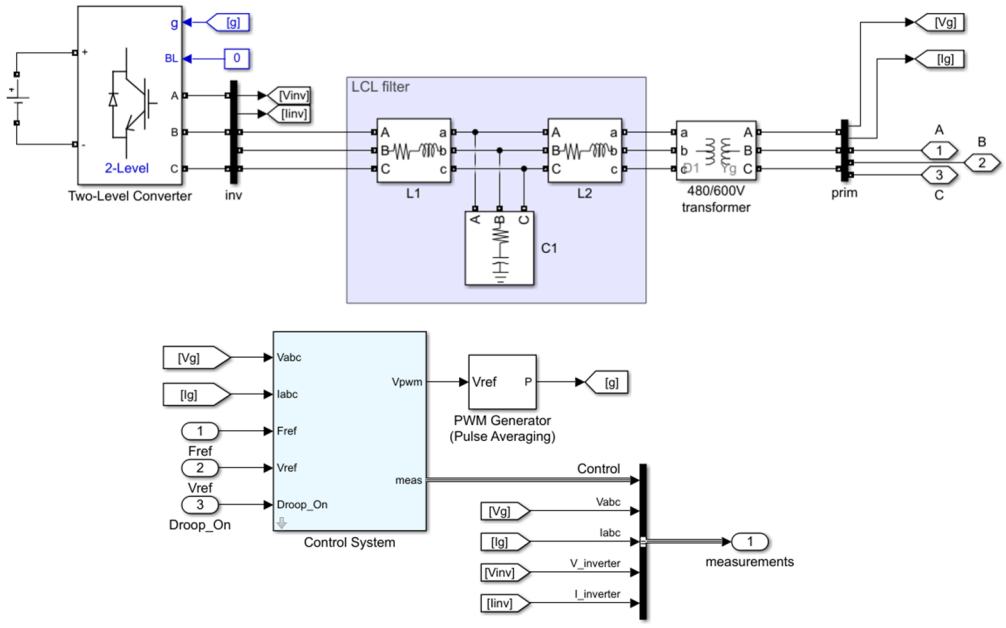

Figure 4.8 Grid Forming Inverter control diagram.

One of the draws back with Simulink is that a limiter and sampling time need to be accurate to emulate if the system goes unstable. In construction of this model, a saturation limit was placed on the frequency between 65Hz and 55Hz, due to the practical nature of this experiment, if the frequency reached those level, we could assume the system is going unstable.

4.4.1 *Case Study 1*

This case study investigates the effects of time delay with a constant load. There will be no changes or external disturbance impacting the system. Moreover, it is anticipated, based on the eigen values obtained in our analysis and the parameters set by the IEEE 1547, there should be a level of instability in the frequency and voltage of the system. Here, we will record the Power, frequency and voltage.

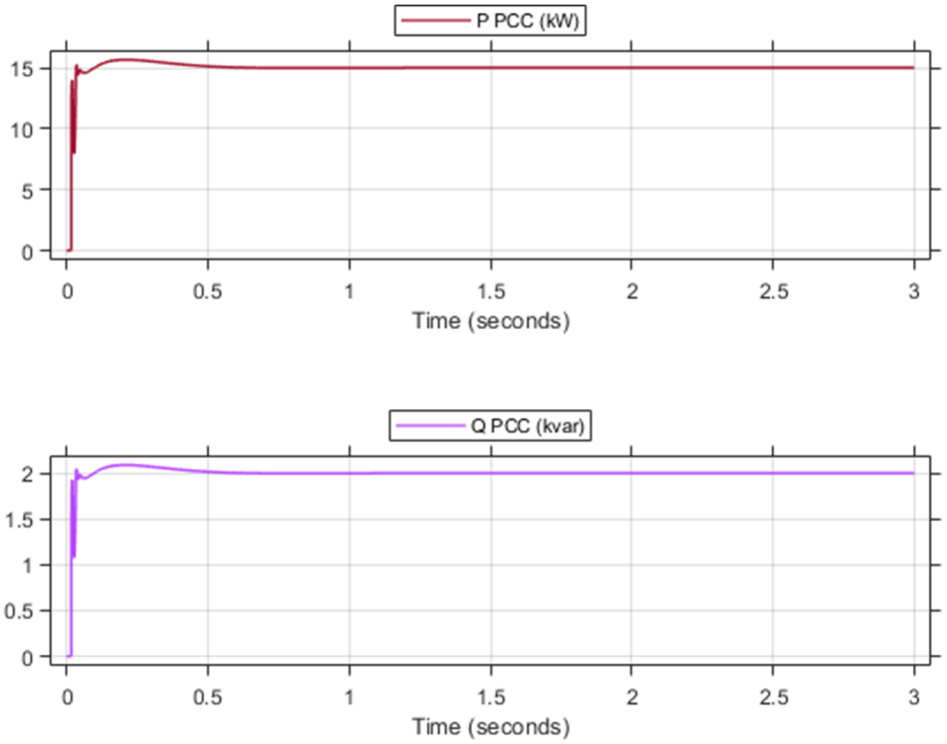

Figure 4.9 Active and Reactive Power @ Td=0, No Load Change

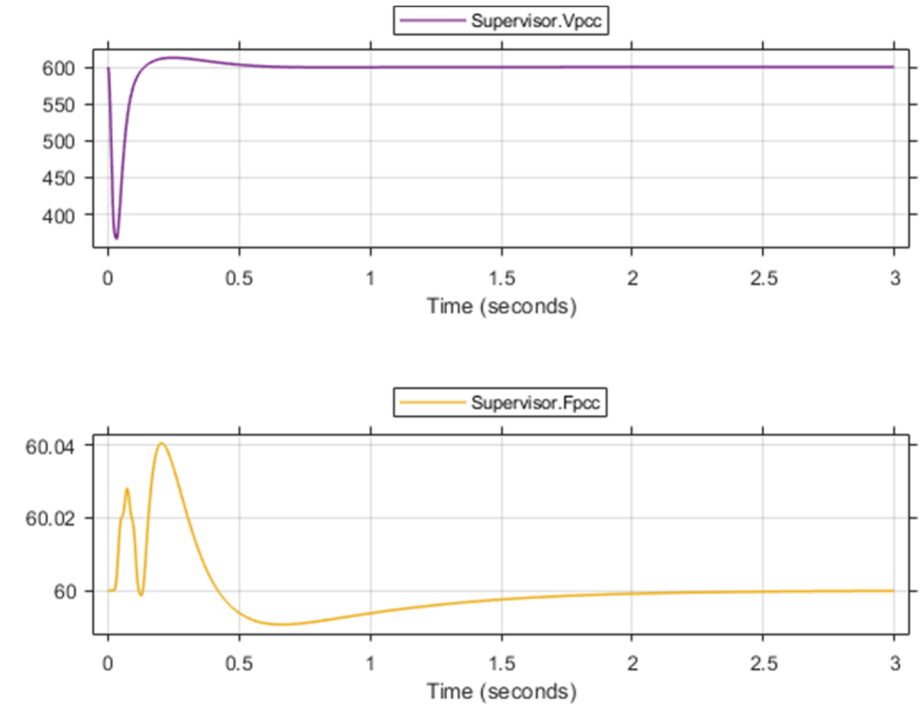

Figure 4.10 Output Voltage and Frequency at PCC @ Td=0, No Load Change

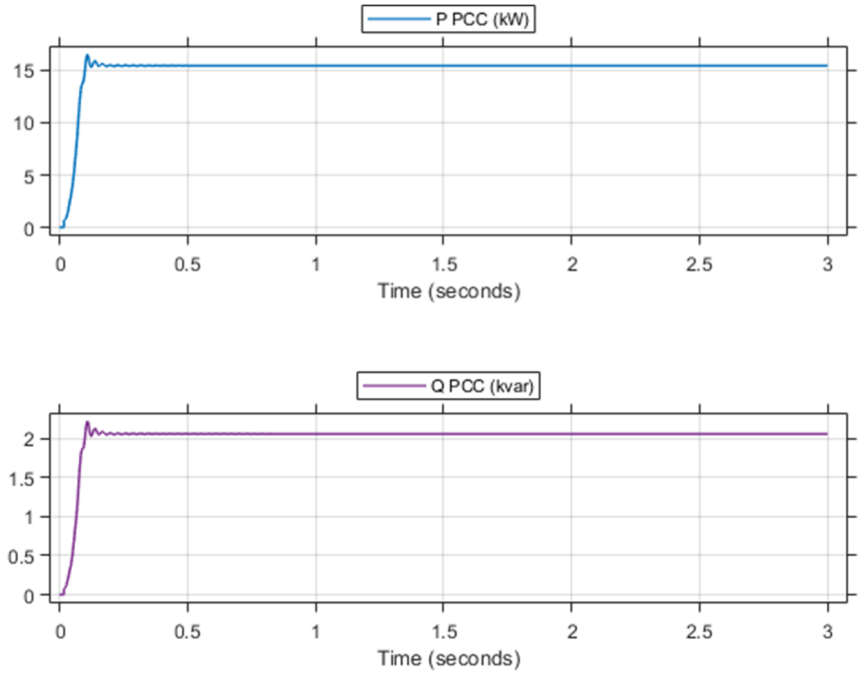

Figure 4.11 Active and Reactive Power @ Td=10ms, No Load Change

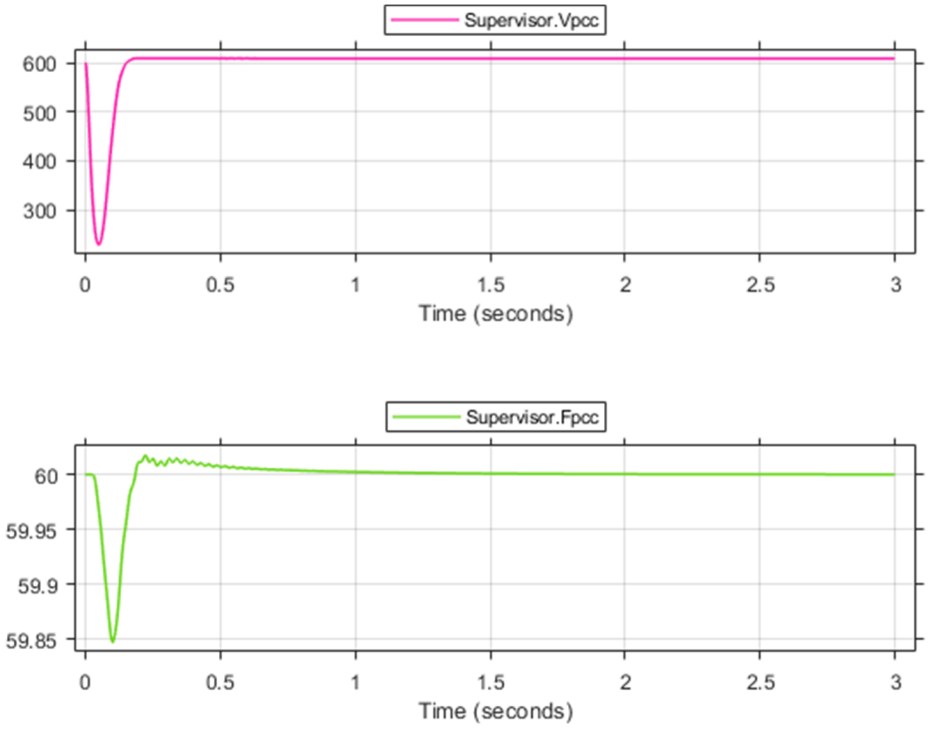

Figure 4.12 Output Voltage and Frequency at PCC @ Td=10ms, No Load Change

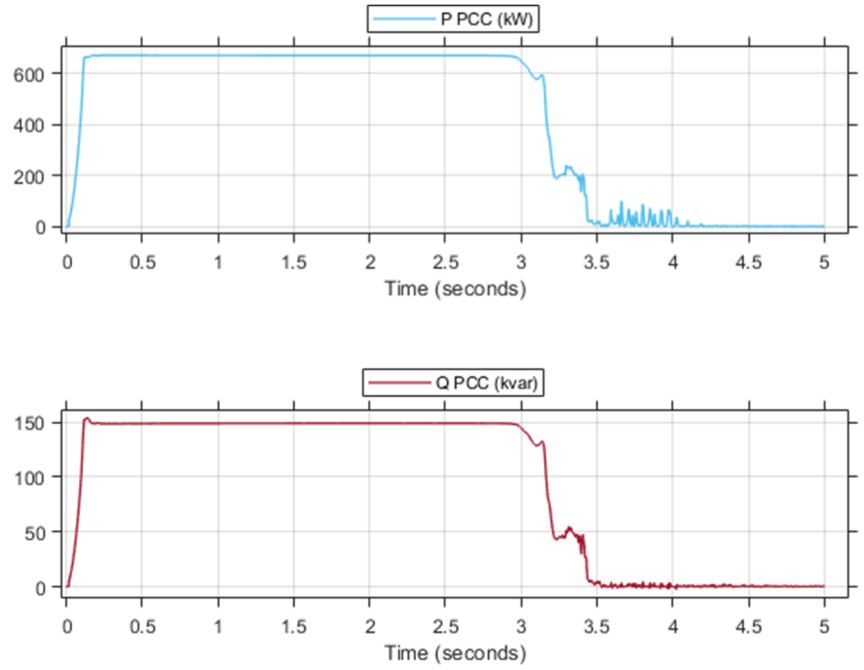

Figure 4.13 Active and Reactive Power @ Td=100ms, No Load Change

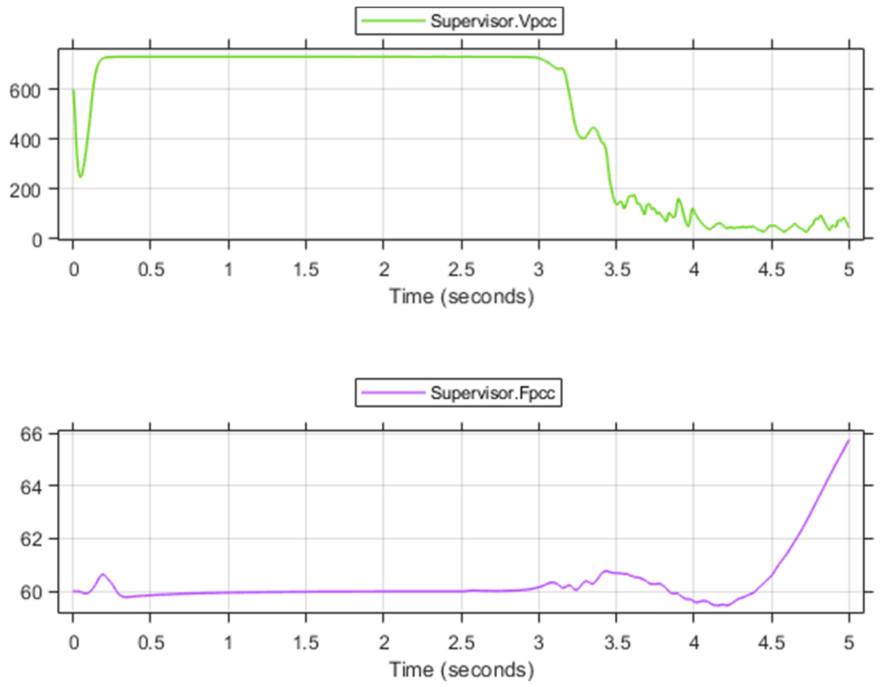

Figure 4.14 Output Voltage and Frequency at PCC @ Td=100ms, No Load Change

4.4.2 *Case Study 2*

In this case the varying load is used, which will increase the load on the grid at t=2s. with a time delay of t=0.

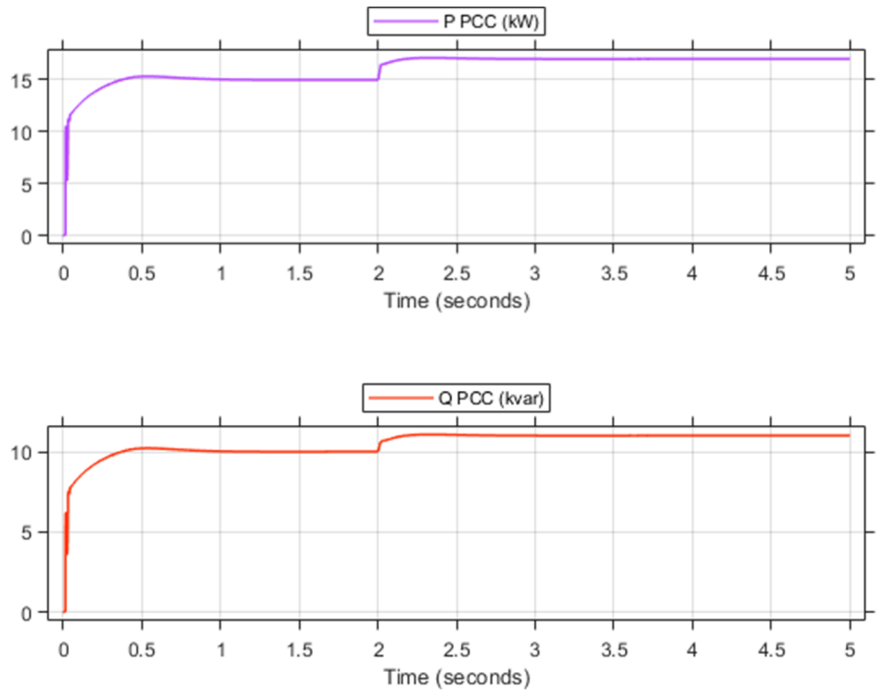

Figure 4.15 Active and Reactive Power at PCC @ Td=0ms, No Load Change

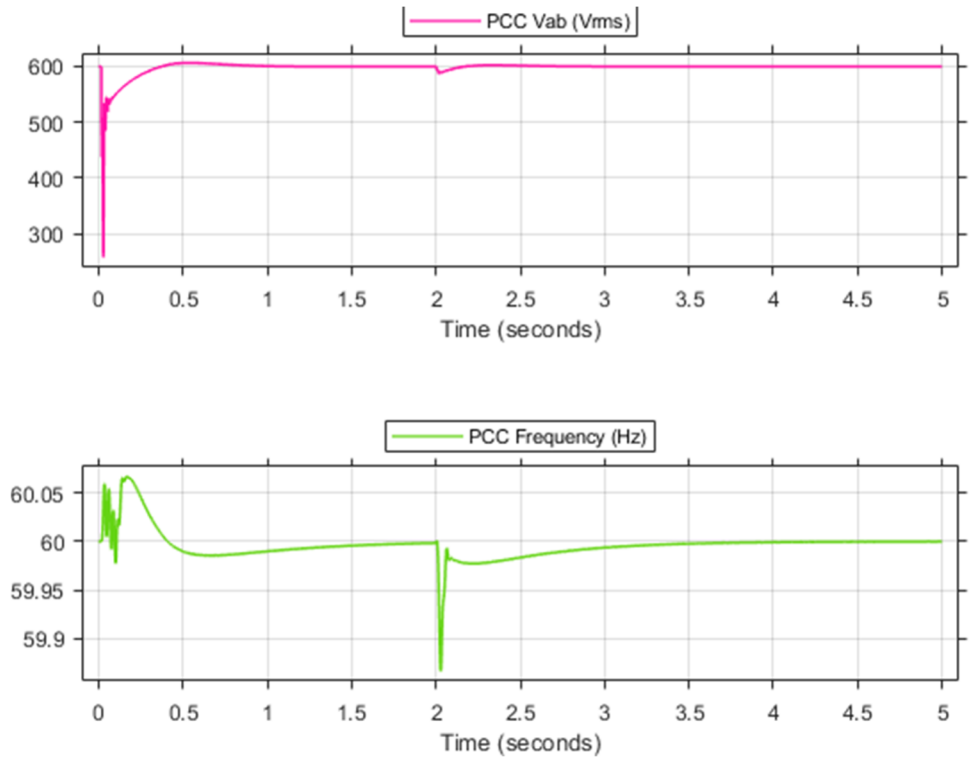

Figure 4.16 Output Voltage and Frequency at PCC @ Td=0ms, No Load Change

Figure 4.13-14 depict the case where the load is varying with a Time delay of 0.s. The load variations start at the two second point. At this junction, the frequency increase slightly to compensate for the load increase of P & Q and remained stable and the frequency decline to 59.8Hz for approximately 0.1s. Per the IEEE 1547, under this condition, this would not affect inverter robustness. With a time, delay of 0, this validates our previous results.

4.4.3 Case Study 3

Case Study 3 looks at the grid forming inverter under fault conditions. Based on our eigen values, and our known knowledge of the IEEE 1547.2018, we know that under fault the inverter needs to be maintain operation for at least 10ms. If this condition is met, we have successfully analysis inverter.

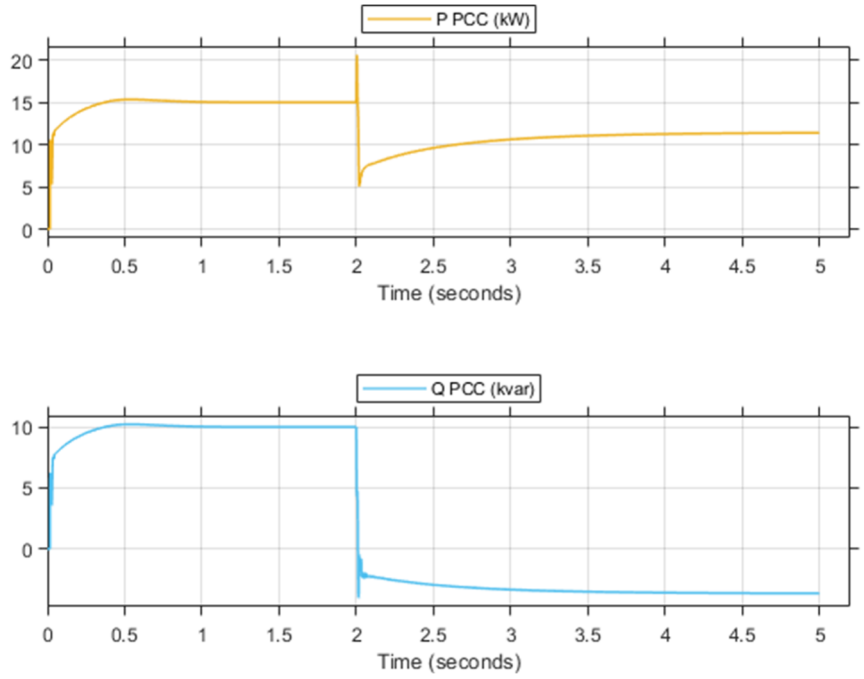

Figure 4.17 Active and Reactive Power at PCC @ Td=0ms, Transient fault

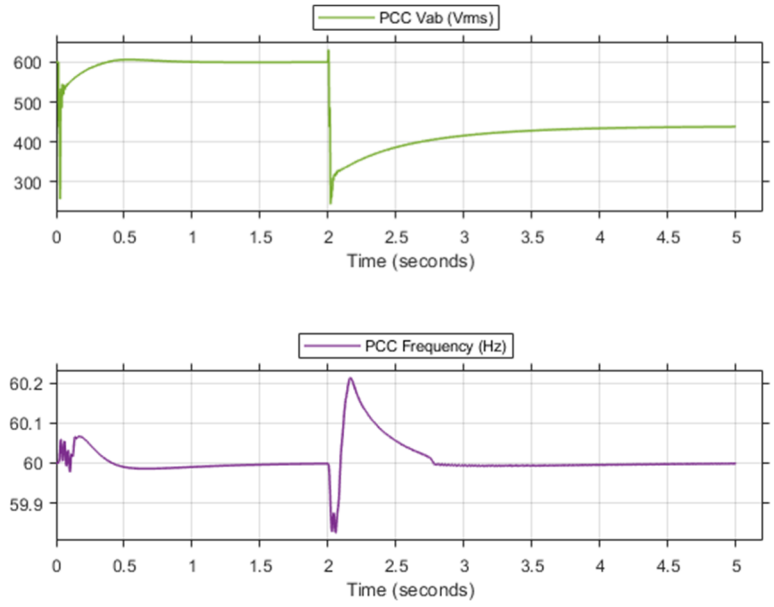

Figure 4.18 Output Voltage and Frequency at PCC @ Td=0ms, Transient fault

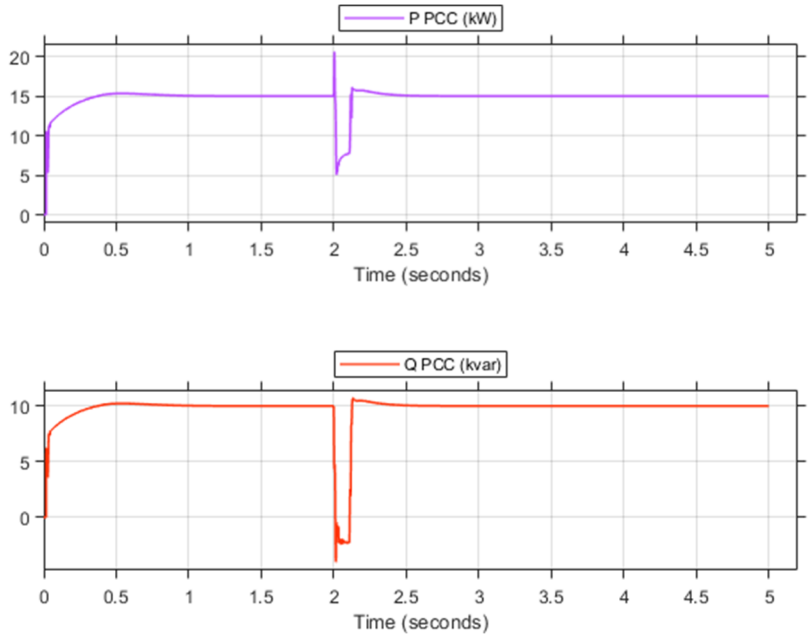

Figure 4.19 Active and Reactive Power at PCC @ Td=0ms, Transient fault

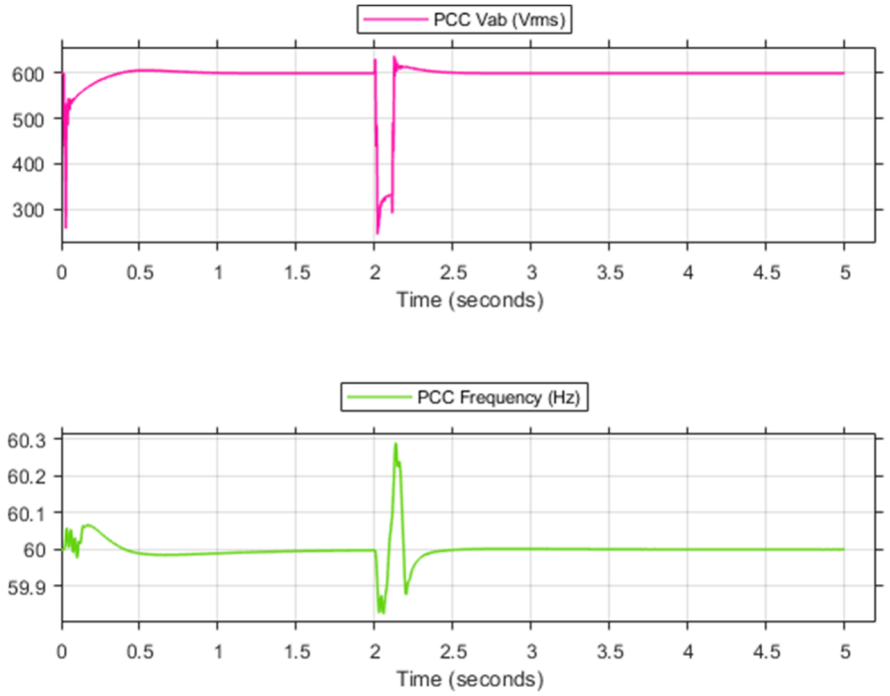

Figure 4.20 Output Voltage and Frequency at PCC @ Td=0ms, Transient fault

4.5 Conclusions

This chapter evaluated the analysis of the time delay impact on the internal stability of the grid forming inverter. As seen in the cases above, it can say, that time delay does have an impact on the stability of the grid forming inverter. Moreover, it shows how robust the internal controllers are can be under different disturbances. Case 1 was used as a benchmark to see the normal operation conditions of the system, without any disturbances. Whereas Case 2 & 3 describes the variations of frequency and voltage under certain disturbance.

CHAPTER 5

PSCAD SIMULATION RESULTS AND MODEL VERIFICATION

5.1 Introduction

With PSCAD you can build, simulate, and model your systems with ease, providing limitless possibilities in power system simulation. Included is a comprehensive library of system models ranging from simple passive elements and control functions to electric machines and other complex devices. PSCAD is widely used to simulate power systems and give a real-world depiction of the outcome from various scenarios. The cases discussed in the previous chapter will be compared to the PSCAD version. To recap, the test model will be the IEEE-9 bus microgrid system with 3 parallel grid forming inverters, as shown in the MATLAB.

The studied microgrid in section 4.4.1 is modelled by MATLAB based on the equations discussed in the modeling chapter (chapter three). The purpose is verifying the accuracy of the modeling implemented in MATLAB by comparing it to the PSCAD detailed modeling. As previously stated, the main components of the system are the PV generator, the battery energy storage, the load demand, the microgrid and the power electronics components. The PV and battery are connected to the microgrid through a DC/AC inverter. Controlling the inverters in a microgrid is a key point. In this modeling, the frequency of a microgrid has been controlled by sending an appropriate control signal to the inverters. Considering the configuration of the system used, the microgrid is divided into two areas. Figure 4.31 shows the way we made the areas in this system. In fact, for the third case, we have two assigned areas where each of them is supposed to take care of its own frequency, so whenever the load is changed in each area, that particular area does its best to control the frequency.

5.2 Detailed Model (In PSCAD) VS Average Model (In MATLAB)

The understudied microgrid is simulated in PDCSAD environment with the detailed component to investigate the accurate result of having a virtual tie line error. However, in order to verify the equation-based modeling (the average model) and compare it with the detailed model, a similar system with average components is implemented in MATLAB software. The main elements affected by the average model are power electronic devices such as inverters. By neglecting the switching action of these converters and assuming the ideal functionality of the three legs inverter, their detailed model is simplified significantly.

Below, some of the results have been compared with the detailed and average model. First, the recovery time in both simulations is shown. Along with the various time delay within the grid forming inverter.

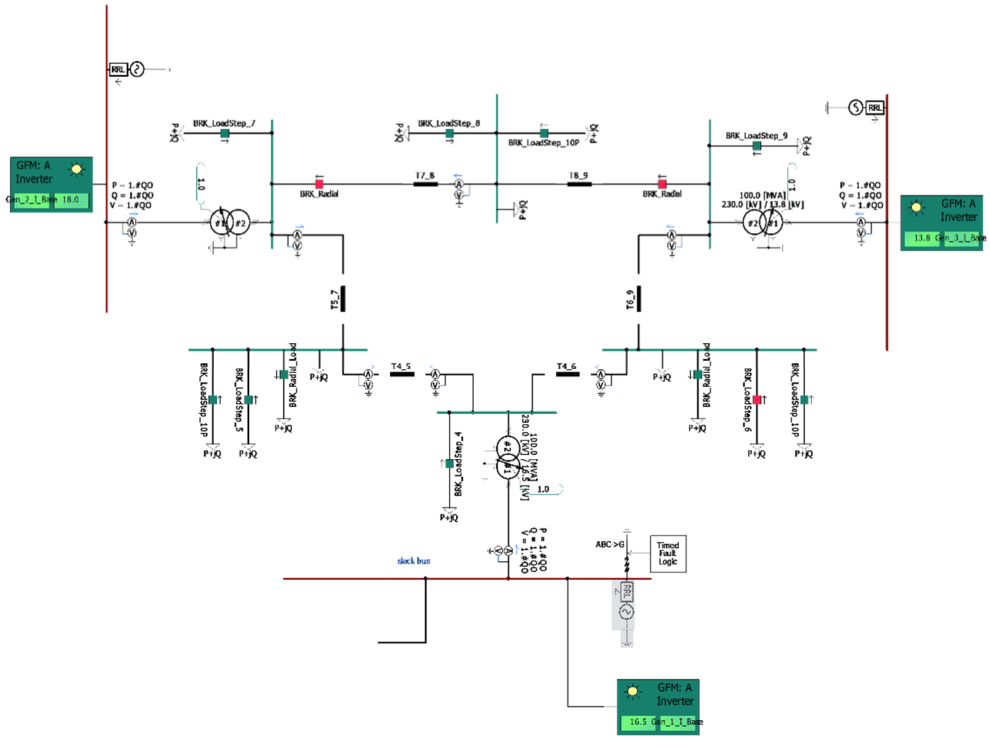

Figure 5.2.1 IEEE 9-Bus System 600MW

We now move to an experimental test using PSCAD. This software allows us to represent the dynamic response of the system. (The original IEEE 9-Bus test system is a standard dynamics test system that has been used for decades to assess new dynamic elements and concepts in power system operations.)This IEEE 9-bus system was modified and tested, which consists of three inverters, 3 GFM, All three devices have an equal rating of 200 MVA, with an assumed ample positive and negative headroom. The loads are modeled as constant power. Device and load specifications are presented in the table 5.1.

Table VI. IEEE 9-Bus System Parameter

Bus	**Device**	**Rating (MVA)**	**Base Voltage(kV)**	**P(MW)**	**Q(Mvar)**
1	GFM 1	200	16.5	66.9	16.1
2	GFM 2	200	18.0	163.6	5.0
3	GFM 3	200	13.8	89.9	-5.0
5	Fixed Load	n/a	230	-125	-50
6	Fixed Load	n/a	230	-90	-30
8	Fixed Load	n/a	230	-100	-35

The Inverters were modified with a time delay component, similar to MATLAB/Simulink on the output of the current controller. Using the CMF time delay tool provided in PSCAD.

The startup for this system obeys the following procedure:

- Energize the system with GFM 1 acting as an ideal source (strict voltage and frequency regulation).

- Ramp up the GFM 2 output to power set points.
- Energize GFM 3 and release the frequency dynamics, then ramp the power set point to the desired quantity;
- (the associated local frequency deviations enable the power flow change, while GFM A ensures the system frequency remains nominal.)
- Apply a disturbance on GFM A Bus at t=4s for 50ms.

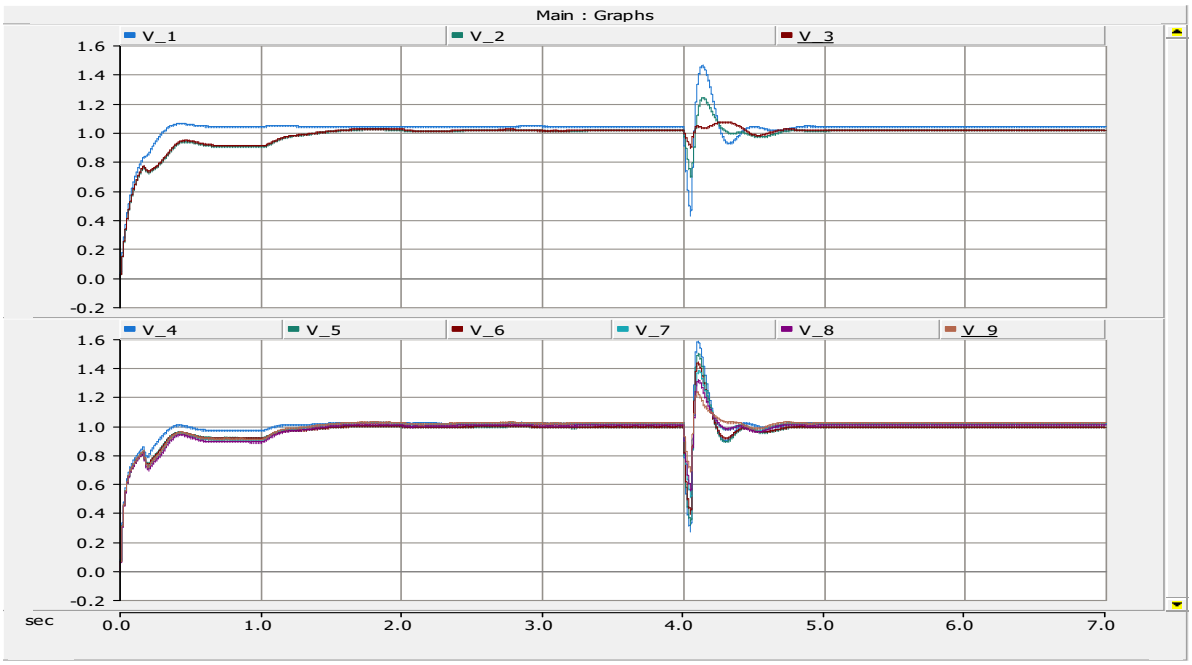

Figure 5.2.2 Case 1: Bus Voltage @ Time delay = 10us

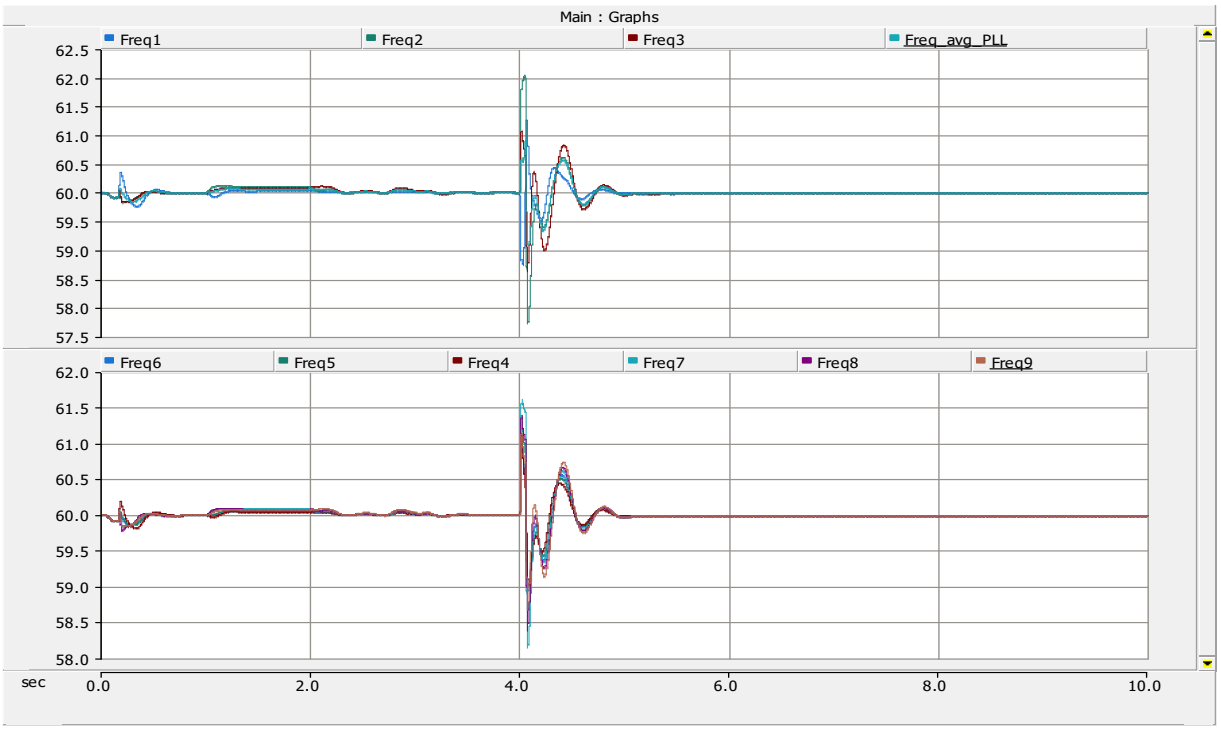

Figure 5.2.3 Case 1: Bus Frequency @ Time delay = 10us

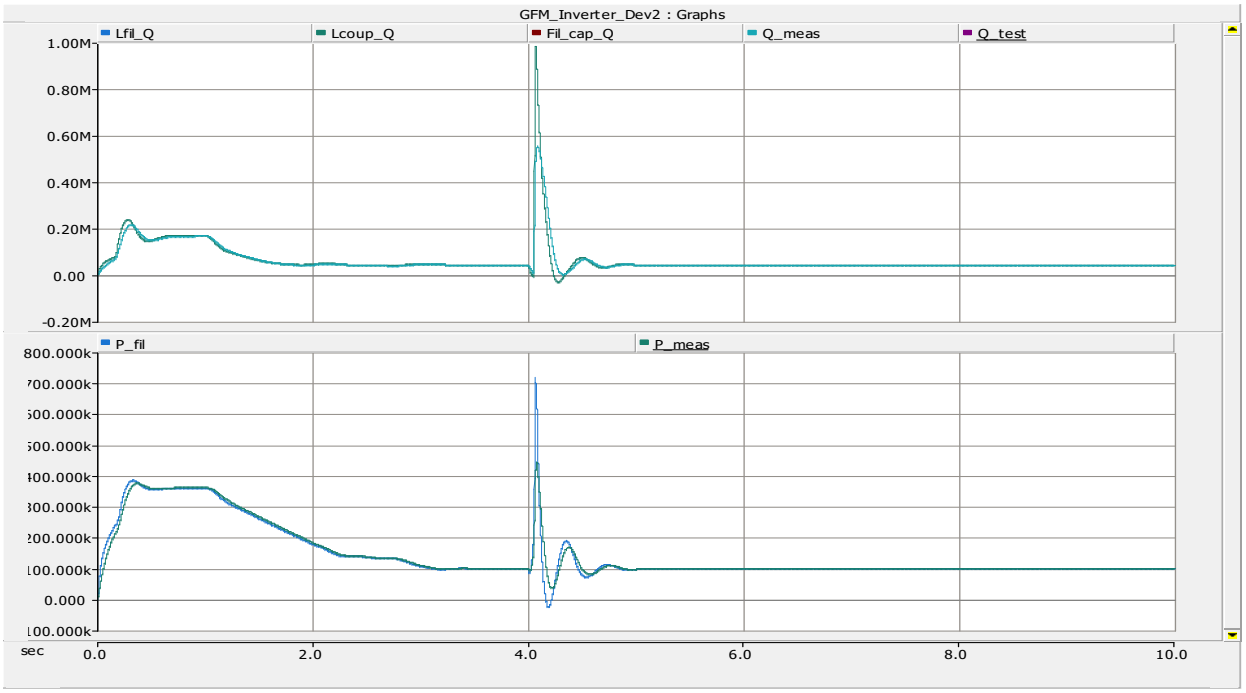

Figure 5.2.4 Case 1: LCL Network @ Time delay = 10us

In case 1, you see the response of the frequency, voltage, and power across the LCL network. In this test case, we induced a fault on bus 1 for 50ms. With a time, delay of 10us. After the fault, the system remains responsive. The fault recovery was very quick and responsive with no issues or irregular dynamics in its usual operation. Along with our corresponding eigen values has shown in the previous chapter.

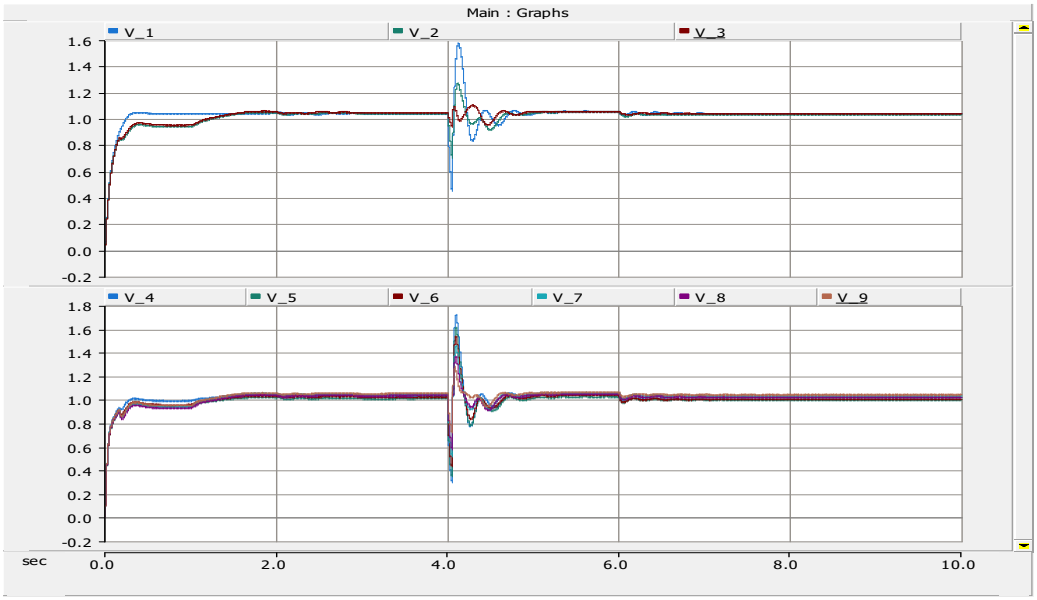

Figure 5.2.5 Case 2: Bus Voltages @ Time delay = 0.1ms

In case 2, you see the response of the frequency, voltage, and power across the LCL network. In this test case, we induced a fault on bus 1 for 50ms. With a time, delay of 10us. After the fault, the system remains responsive. The fault recovery remained quick and responsive with no issues or irregular dynamics response in its usual operation. As you can see from our eigen value spectrum in chapter 4, they are stable as well.

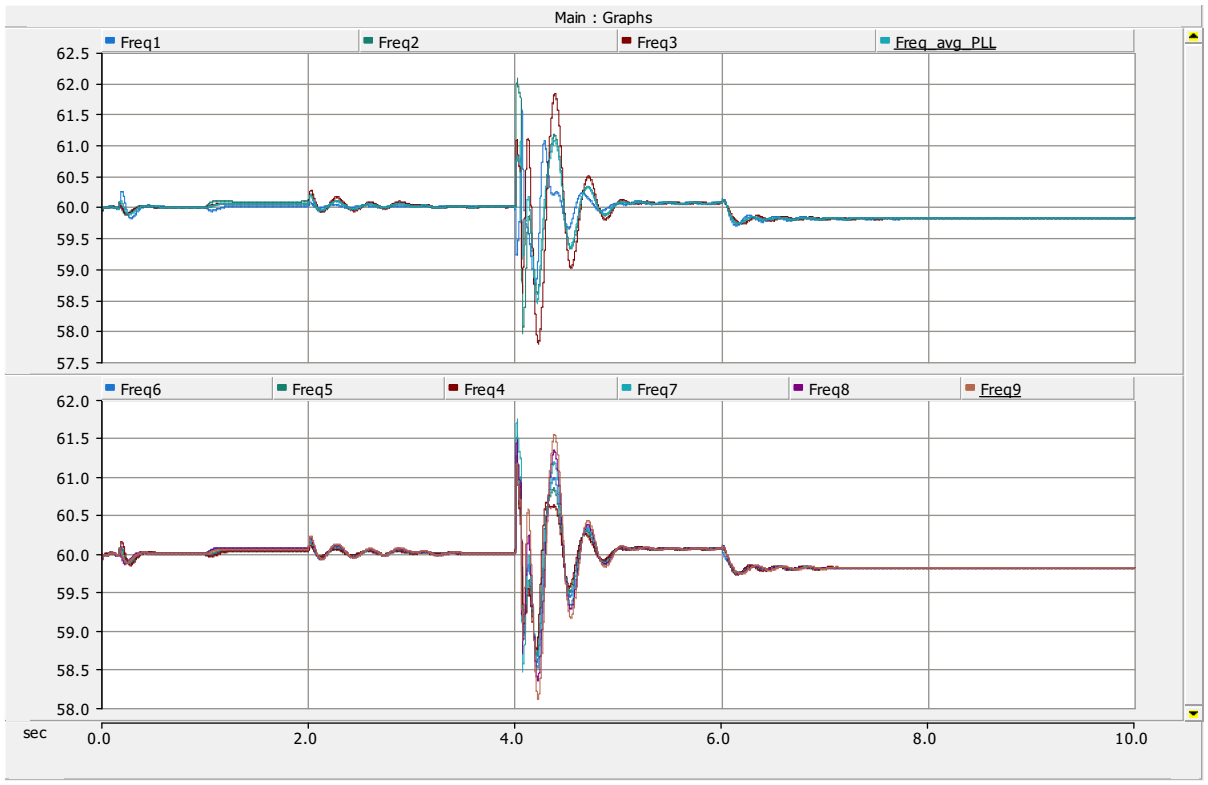

Figure 5.2.6 Case 2: Bus Frequency @ Time delay = 0.1ms

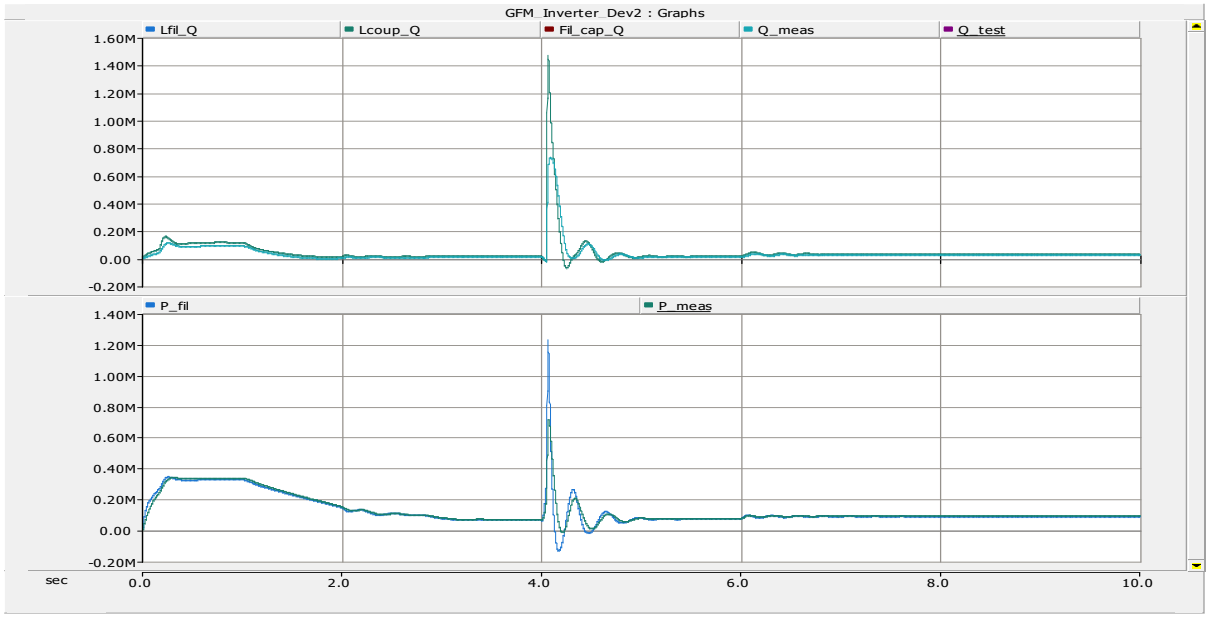

Figure 5.2.7 Case 2: LCL Network @ Time delay = 0.1ms

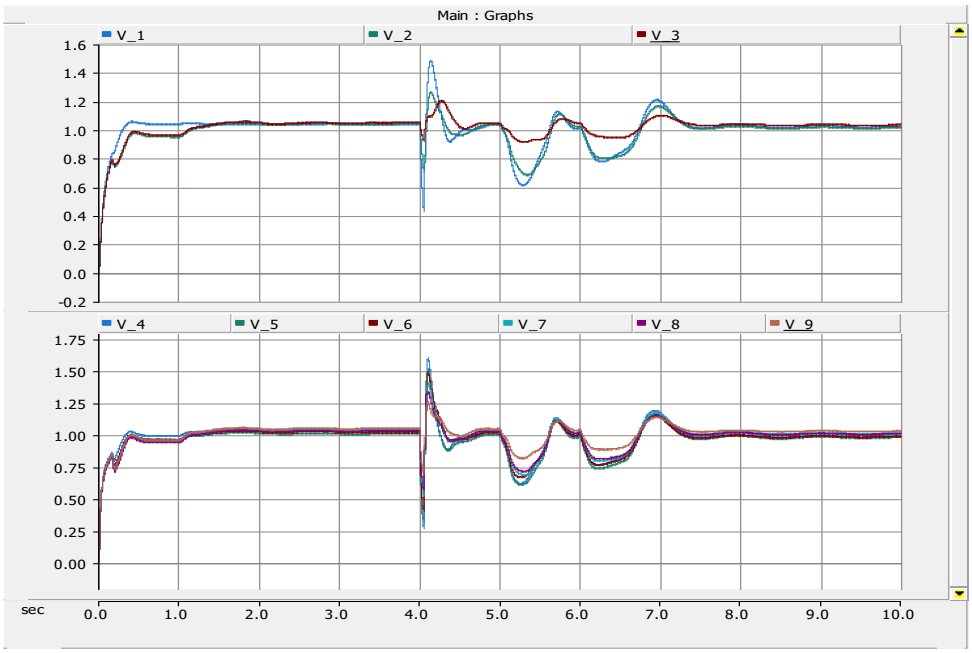

Figure 5.2.8 Case 3: Bus Voltages @ Time delay = 0.5ms

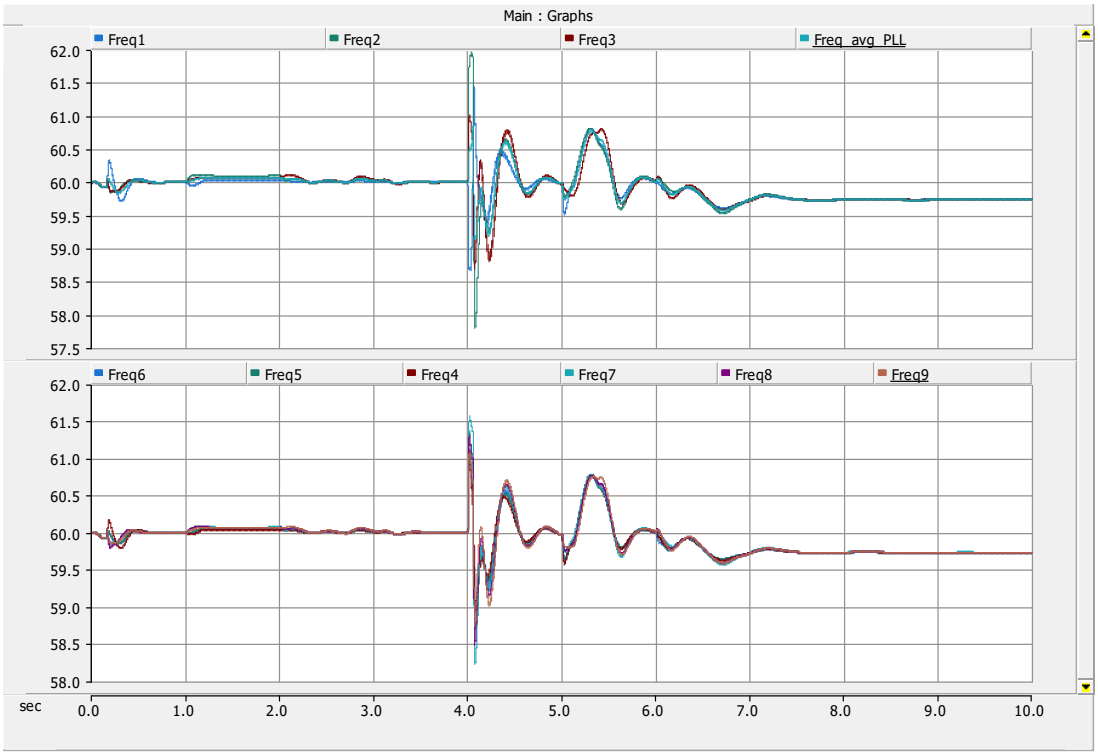

Figure 5.2.9 Case 3: Bus Frequency @ Time delay = 0.5ms

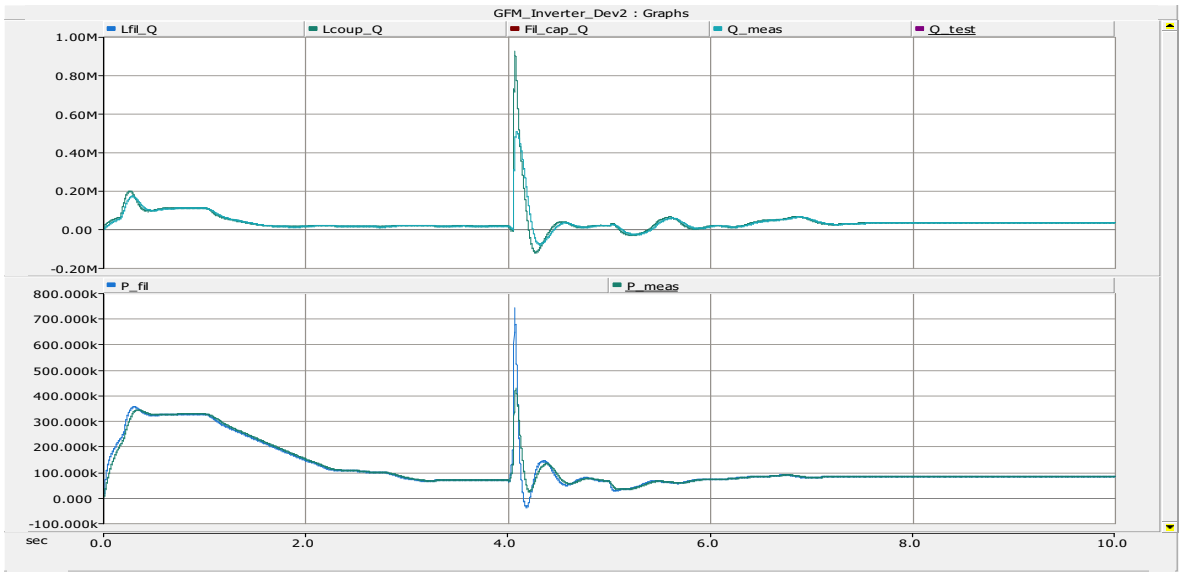

Figure 5.2.10 Case 3: LCL Network @ Time delay = 0.5ms

In this test case a time delay of 0.5ms was applied. After the fault, the system took a much longer time (3s) to reach its nominal values. But remained in a reasonable range. With no issues or irregular dynamics in its usual operation. Looking at our eigen values, we notice a few modes are right near the zero-crossing in chapter 4. Although for a linear system, this can still be classified as stable. However, in a non-linear system, there are numerous variables that can affect the overall responsiveness of the system. In our test case on PSCAD, we are modelling a non-linear system, thus our system is still responsive.

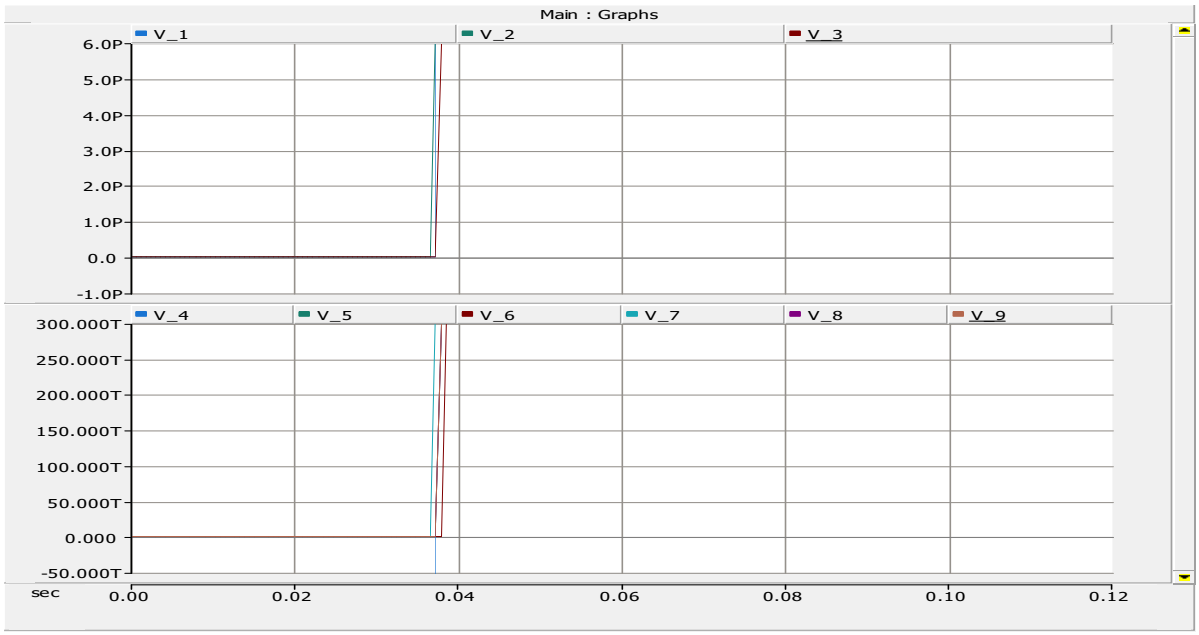

Figure 5.2.11 Case 4: Bus Voltages @ Time delay > 0.5ms

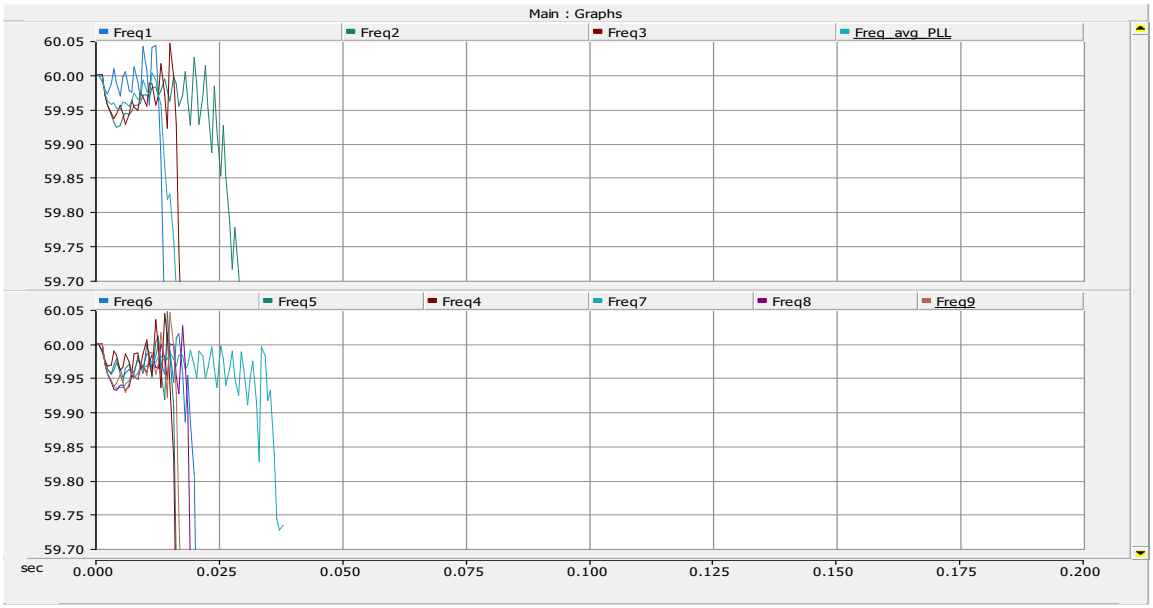

Figure 5.2.12 Case 4: Bus Frequency @ Time delay > 0.5ms

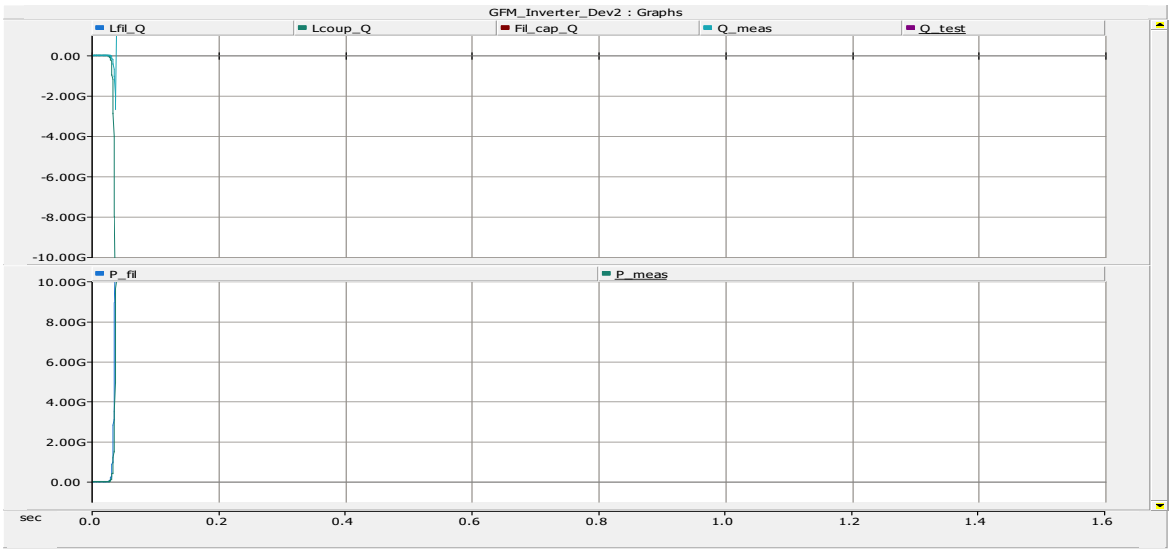

Figure 5.2.13 Case 4: LCL Network @ Time delay > 0.5ms

In this test case, the time delay is greater than 0.5ms. At this junction, we see a significant change in the frequency and voltage. By referring to our eigenvalue spectrum, It can be said or inferred that our results were consistent with the dynamic response of these values at a time delay over 0.5ms. In analyzing this dynamic system. We see that our Power across LCL Network experiences a huge dynamic response, which cascaded to the frequency and voltage. *(Causing our voltage to reach our DC-link limit. This then affected our frequency).* At this point, the GFM was not responding to the inputs from the voltage of the coupling inductor when the time delays were greater than 0.5ms. This analysis was consistent with our findings in MATLAB/Simulink. Other test cases were performed on PSCAD, but these results are pertinent for our general conclusion.

CHAPTER 6

CONCLUSIONS AND FUTURE WORK

6.1 Conclusions

The objective of this thesis is to provide a better understanding of ride through fault capabilities of Grid Forming Inverter (GFM) tied into the generation side of the power grid when using control functions. Furthermore, to investigate the robustness of implementing time delay with a PLL system within the control settings for grid forming inverters. To this end, to identify the contributing factors that affects the stability of the time delay to better design and future models of GFMs. As discussed, the microgrid is a potential solution for future distributed generation systems. It aggregates many distributed energy resources (DER), like renewable sources, and loads as an autonomous region. However, controlling a microgrid is still a complex issue and many proposed solutions, are only based on locally measured signals without any communications; thus, it is difficult to achieve global optimization. A comprehensive state space model of a microgrid including the PLL and time delay between the controllers of the VSI inverters is presented.

The effect of the nominal time delay agreement and the participating factors that's affects the stability of the frequency set-point for VSI inverters and active and reactive power set-points and voltages was founded. Variations of the time delay and application of IEEE-1547 was considered all through the modeling which is then used to investigate the small signal stability and the effect of proposed time delay VSI model. Single bus system with three parallel inverters was used to illustrate the effectiveness of this approach.

The system model was defined in chapter 3. This included the state space model of the Power controller, voltage controller, current controller, time delay, phase lock loop, LCL system, network lines and loads. Their state variables were defined into a total system equation.

The stability results presented at chapter 4 indicate that the modeling method can be used to analyse the stability of the microgrid primary control. In addition, the simulation results show the controller successfully coordinates the multiple inverters under challenging load conditions while managing their individual constraints and internal stability. The main purpose of this approached was to define the participating factors that affect the robust stability of the inverter using MATLAB/Simulink. This is important, to identify what elements and variables in the utility control, that can be configured to improve the stability of the Grid Forming Inverter. As anticipated, the variation of the droop control, plays a key factor. As stated in the introduction implementing a controller, constitute to a form of delay. If it found that the output current and voltage plays a vital role in the robust stability of the grid forming inverter. Consequently, this means that the output line inductor and capacitor play a significant role in this. In chapter 4, this concept was tested in Simulink on a single bus system. Where the output inductor and capacitor varied among the system. By increasing load and decreasing loads. Moreover, inducing a system fault to test the ride-through capabilities of this inverter while varying the time delay.

The simulation result in the previous chapter shows the effectiveness of the algorithm in case of load changes in the system. As founded, the time delay of the controller must be within 0s to 0.05s, to maintain a stable inverter. Although at 0.05s, it can be seen, that the system is somewhat stable but due to the external disturbance they may impact the system with the eigen values being so close to 0. Any disturbance can be more than enough to run the inverter unstable.

6.2 Recommendation for Future Work

Based on the work presented, the following future work is proposed

- Use of artificial intelligence and data-driven controllers can be studied. Modeling and stability study of conventional controllers is tedious work. And given the complexity of an inverter-based system, a data-driven approach can be used to model such a system so that it can encompass intricate details of the system which are often overlooked while mathematical modeling. Such a model can be used for stability study purposes.
- The future work could also include the effects of time delays in automatic protection equipment (relay coordination) since breaker reclosures introduce a switched behaviour in the system dynamics.
- A analysis of the different factor that affects the internal stability and robustness of the grid forming inverter, such as the output inductor, droop controller setting and PLL implementations.
- Developing programming tools for modeling and analysis of the electric system which can visualize the theoretical concept of smart grids control and implementation.
- Improving the microgrid's intelligent operation by integrating smart devices into the system and developing smart grids by utilizing communication-based multi-agent systems
- Improve the microgrid robust strength in fault clearing by adding a current limiting device to increase their ride-through capabilities.
- Develop model simulations in PSCAD on a more robust power system network. This to provide a more consistent results to emulate the inverter behaviour.

APPENDIX A

MATLAB/Simulink SCRIPTS

The MATLAB scripts are written below for the selected case studies. This Appendix contains the MATLAB/Simulink of parallel three-phase microgrid inverter models.

A.1 MATLAB Simulink main.m File

REFERENCE

1. “Final Report on the August 14, 2003 Blackout in the United States and Canada: Causes and Recommendations”, U.S. – Canada Power System Outage Task Force, April 5, 2004.

2. D. B. Rathnayake *et al*., "Grid Forming Inverter Modeling, Control, and Applications," in *IEEE Access*, vol. 9, pp. 114781-114807, 2021, doi: 10.1109/ACCESS.2021.3104617.

3. Y. Lin, J. H. Eto, B. B. Johnson, J. D. Flicker, R. H. Lasseter, H. N. Villegas Pico, G.-S. Seo, B. J. Pierre, and A. Ellis, “Research roadmap on grid-forming inverters,” *Research Roadmap on Grid-Forming Inverters (Technical Report) | OSTI.GOV*, 11-Nov-2020. [Online]. Available: https://www.osti.gov/biblio/1721727.

4. J. Matevosyan et al., "A Future With Inverter-Based Resources: Finding Strength From Traditional Weakness," in IEEE Power and Energy Magazine, vol. 19, no. 6, pp. 18-28, Nov.-Dec. 2021, doi: 10.1109/MPE.2021.3104075.

5. D. Pattabiraman, R. H. Lasseter. and T. M. Jahns, "Comparison of Grid Following and Grid Forming Control for a High Inverter Penetration Power System," 2018 IEEE Power & Energy Society General Meeting (PESGM), Portland, OR, USA, 2018, pp. 1-5, doi: 10.1109/PESGM.2018.8586162.

6. W. Du, K. P. Schneider, F. K. Tuffner, Z. Chen and R. H. Lasseter, "Modeling of Grid-Forming Inverters for Transient Stability Simulations of an all Inverter-based Distribution System," 2019 IEEE Power & Energy Society Innovative Smart Grid Technologies Conference (ISGT), Washington, DC, USA, 2019, pp. 1-5, doi: 10.1109/ISGT.2019.8791620..

7. R. H. Lasseter, J. H. Eto, B. Schenkman, J. Stevens, H. Vollkommer, D. Klapp, et al., "CERTS Microgrid Laboratory Test Bed," IEEE Transactions on Power Delivery, vol. 26, pp. 325-332, 2011.

8. R. Majumder, B. Chaudhuri, A. Ghosh, R. Majumder, G. Ledwich, and F. Zare, ``Improvement of stability and load sharing in an autonomous microgrid using supplementary droop control loop," IEEE Trans. Power Syst., vol. 25, no. 2, pp. 796808, May 2010.

9. C. -T. Lee, C. -C. Chu and P. -T. Cheng, "A new droop control method for the autonomous operation of distributed energy resource interface converters," 2010 IEEE Energy Conversion Congress and Exposition, Atlanta, GA, USA, 2010, pp. 702-709, doi: 10.1109/ECCE.2010.5617936.

10. W. Du et al., "A Comparative Study of Two Widely Used Grid-Forming Droop Controls on Microgrid Small-Signal Stability," in IEEE Journal of Emerging and Selected Topics in Power Electronics, vol. 8, no. 2, pp. 963-975, June 2020, doi: 10.1109/JESTPE.2019.2942491.

11. X. Niu, H. Ye, Y. Liu and X. Liu, "Padé approximation based method for computation of eigenvalues for time delay power system," 2013 48th International Universities' Power Engineering Conference (UPEC), Dublin, Ireland, 2013, pp. 1-4, doi: 10.1109/UPEC.2013.6714971.

12. B. Shoeiby, D. G. Holmes, B. P. McGrath and R. Davoodnezhad, "Dynamics of droop-controlled microgrids with unequal droop response times," *2013 Australasian Universities Power Engineering Conference (AUPEC)*, Hobart, TAS, Australia, 2013, pp. 1-6, doi: 10.1109/AUPEC.2013.6725485.

13. L. Marin, A. Tarrasó, I. Candela and P. Rodriguez, "Stability Analysis of a Droop-Controlled Grid-Connected VSC," *2018 IEEE Energy Conversion Congress and Exposition (ECCE)*, Portland, OR, USA, 2018, pp. 4161-4167, doi: 10.1109/ECCE.2018.8558126.

14. Y. He, M. Wu, and J. H. She, “Delay-dependent stability criteria for linear systems with multiple time delays,” Proc. Inst. Elect. Eng., Control Theory Appl., vol. 153, no. 4, pp. 447–452, Jul. 2006.

15. S. Y. Xu and J. Lam, “On equivalence and efficiency of certain stability criteria for time-delay systems,” IEEE Trans. Automat. Control, vol. 52, no. 1, pp. 95–101, Jan. 2007.

16. R. Olfati-Saber and R. M. Murray, "Consensus problems in networks of agents with switching topology and time-delays," in *IEEE Transactions on Automatic Control*, vol. 49, no. 9, pp. 1520-1533, Sept. 2004, doi: 10.1109/TAC.2004.834113.

17. Henrique Jos´e Avelar, Wanderley Alves Parreira, Jo˜ao Batista Vieira, Luiz Carlos Gomes de Freitas, and Ernane Antˆonio Alves Coelho. A state equation model of a single-phase grid-connected inverter using a droop control scheme with extra phase shift control action. IEEE Transactions on Industrial Electronics, 59(3):1527–1537, 2012.

18. Amirnaser Yazdani and Reza Iravani. Voltage-sourced converters in power systems: modeling, control, and applications. John Wiley & Sons, 2010.

19. N. Pogaku, M. Prodanovic and T. C. Green, "Modeling, Analysis and Testing of Autonomous Operation of an Inverter-Based Microgrid," in *IEEE Transactions on Power Electronics*, vol. 22, no. 2, pp. 613-625, March 2007, doi: 10.1109/TPEL.2006.890003

20. Hongxia Wu, K. S. Tsakalis and G. T. Heydt, "Evaluation of time delay effects to wide-area power system stabilizer design," in IEEE Transactions on Power Systems, vol. 19, no. 4, pp. 1935-1941, Nov. 2004, doi: 10.1109/TPWRS.2004.836272.

21. V. Kaura and V. Blasko, "Operation of a phase locked loop system under distorted utility conditions," in IEEE Transactions on Industry Applications, vol. 33, no. 1, pp. 58-63, Jan.-Feb. 1997, doi: 10.1109/28.567077.

22. Hessam Keshtkar Vanashi, Farideh Doost Mohammadi, Vishal Verma, Jignesh Solanki, and Sarika Khushalani Solanki. Hierarchical multi-agent based frequency and voltage control for a

microgrid power system. International Journal of Electrical Power & Energy Systems, 135:107535, 2022.

23. G. D´ýaz, C. Gonz´alez-Mor´an, J. G´omez-Aleixandre and A. Diez, “Complex-valued state matrices for simple representation of large autonomous microgrids supplied by PQ and Vf generation,” IEEE Trans. on Power Systems, vol. 24, no. 4, pp. 1720–1730, Nov. 2009.

24. Kwonhue Choi; Huaping Liu, "Phase-Locked Loop and Synchronization," in Problem-Based Learning in Communication Systems Using MATLAB and Simulink , IEEE, 2016, pp.135-150, doi: 10.1002/9781119060239.ch13.